2014

A Study on Atmospheric and Oceanic Processes in the North Indian Ocean

Clifford Steven Felton
University of South Carolina - Columbia

A STUDY ON ATMOSPHERIC AND OCEANIC PROCESSES IN THE NORTH INDIAN OCEAN

by

Clifford S. Felton

Bachelor of Science
North Carolina State University, 2012

Submitted in Partial Fulfillment of the Requirements

For the Degree of Master of Science in

Marine Science

College of Arts and Sciences

University of South Carolina

2014

Accepted by:

Subrahmanyam Bulusu, Director of Thesis

George Voulgaris, Reader

Venkat Lakshmi, Reader

Lacy Ford, Vice Provost and Dean of Graduate Studies

DEDICATION

To Jesus Christ my Lord and Savior who paid the price from my sins, and whose words and Spirit granted me the strength, patience, and endurance to complete this work.

ACKNOWLEDGEMENTS

There are several people I would like to thank for all of their help and support in accomplishing this project, without which none of this work would have been possible. I would like to thank my advisor, Dr. Subrahmanyam Bulusu, who took me into his lab and helped shape and mold my understanding of oceanography as well as my capabilities as a researcher. Thanks to my committee members, Dr. George Voulgaris and Dr. Venkat Lakshmi, the Marine Science Directors Dr. Clauida Benitez-Nelson and Dr. Ron Benner, the Graduate Directors Dr. David Barbeau and Dr. Scott White, and all the faculty members whom I took classes with as a graduate student. Additionally, I would like to thank Drs. V.S.N. Murty, Chief Scientist, CSIR-National Institute of Oceanography Regional Centre, Visakhapatnam, India and Jay F. Shriver, Oceanographer, Naval Research Laboratory, Stennis Space Center, Mississippi, for serving as co-authors and providing assistance throughout the publication process. Special thanks to my lab mates Ebenezer Nyadrjo, Gary Grunseich, Matt Nienhaus, Nicki Button, John Bartlett and Cameron George as well as all of my other friends for getting me through the difficult periods of graduate life, especially William Bledsoe and Andy Rekers. Thanks to my parents, Joyce and Steven Felton for their guidance and wisdom, and special thanks to Angela Popovich and her family, who opened their home to me many times during my studies.

ABSTRACT

Studies on oceanic and atmospheric processes in the Indian Ocean are an active and important area of scientific research. Understanding how intraseasonal and interannual variations impact both the ocean and atmosphere will aid in delineating potential feedback mechanisms and global teleconnections. Thanks to recent efforts focused on expanding observational capabilities and developing models for this region, researchers have been able to begin investigating atmospheric and oceanic processes in the Indian Ocean.

This study focuses on the impact of the El Niño Southern Oscillation (ENSO) on tropical cyclone activity over the Bay of Bengal (BoB) and on developing a method for estimating the barrier layer thickness (BLT) in the Indian Ocean from satellite observations. National Center for Environmental Prediction (NCEP-2) and Simple Ocean Data Assimilation (SODA) reanalysis data are used to investigate the alterations in atmospheric and oceanic conditions that impact tropical cyclones during ENSO events over a 33-year time frame (1979-2011). Atmospheric conditions are shown to be more favorable for tropical cyclone development during La Niña over the BoB due to the favorable alteration of large-scale wind, moisture, and vorticity distributions.

By combining multiple satellite observations, including the recently launched Soil Moisture and Ocean Salinity (SMOS) and Aquarius SAC-D salinity missions, BLT estimates for the Indian Ocean are generated with the use of a multilinear regression model (MRM). The performance of the MRM is evaluated for the Southeast Arabian Sea

(SEAS), Bay of Bengal (BoB), and Eastern Equatorial Indian Ocean (EEIO) where barrier layer formation is most rigorous. Results from the MRM suggest that salinity measurements obtained from Aquarius and SMOS can be useful for tracking and predicting the BLT in the Indian Ocean.

TABLE OF CONTENTS

LIST OF TABLES

LIST OF FIGURES

CHAPTER 1

INTRODUCTION

The importance of the Indian Ocean on local and global processes has only recently begun to be investigated. This ocean basin is unique when compared to the Atlantic and Pacific due to the presence of the Asian continent to the north that blocks northward heat transport by ocean currents. High topographic features (such as the Himalayas and the Tibetan Plateau) also allow for the world's strongest monsoon system to develop. This lack of a northward polar connection causes atmospheric and ocean conditions to be strongly linked to the monsoon cycle. Seasonally reversing monsoonal winds cause ocean currents and weather patterns to vary throughout the North Indian Ocean. During the Indian summer monsoon (June-September), winds blow from the southwest causing ocean currents to generally flow towards the east. Conversely during the winter monsoon season (December-March), winds reverse, blowing from the northeast driving westward flowing surface currents.

In addition to the seasonal monsoon cycle, the ENSO (El Niño Southern Oscillation) also influences atmospheric and oceanic conditions in the North Indian Ocean. The ENSO is characterized by anomalous sea surface temperatures (SSTs) in the central Pacific Ocean that cause alterations in global weather patterns through the Walker Cell (Bjerknes 1969). While ENSO is primarily a Pacific Ocean phenomenon, oceanic and atmospheric conditions are altered in the Indian Ocean as well (Camargo et al. 2007; Hong et al. 2010). During El Niño, convection is reduced over the eastern Indian Ocean

due to the eastward displacement of the Walker Cell, while during La Niña convection is enhanced over the eastern Indian Ocean due to the strengthening of the Walker Cell circulation. The shift in convection patterns during El Niño years can cause the summer monsoon to fail (Ashok et al. 2001).

Indian Ocean Dipole (IOD) is another large-scale feature that impacts the Indian Ocean. Similar to ENSO, the IOD is also characterized by anomalous SSTs. During the positive phase of the IOD, higher SSTs in the western Indian Ocean drive easterly winds that cause cooler SSTs and decreased cloud cover along the Sumatran coastline (Saji et al. 1999). The alteration in winds (and wind stress) also generates anomalous equatorial wave activity (Rossby and Kelvin waves), which alter ocean circulation patterns and the thermocline depth throughout the Indian Ocean (McPhaden and Nagura 2013).

Tropical cyclone (TC) activity over the BoB is strongly tied to the monsoon cycle, resulting in a unique bimodal distribution of occurrences. High sea surface temperatures (SSTs) and the northward propagation of the Indian summer monsoon causes TCs to form from March-May while enhanced moisture drives the second peak from October-December (Yanase et al. 2012; Z Li et al. 2013). In addition to the influence of the seasonal monsoon cycle on TC activity, ENSO also impacts TC development in the BoB (Singh et al. 2001; Girishkumar and Ravichandran 2012). ENSO causes shifts in oceanic and atmospheric conditions in the Indian Ocean that cause the environment to become more or less conducive for TC development. Understanding the environmental changes forced by ENSO is crucial for improving TC forecasts in this vulnerable region where eight of the top ten deadliest tropical cyclones have occurred.

On the oceanic side, the tropical Indian Ocean experiences the most rigorous barrier layer (BL) formation of the ocean basins in response to strong upper ocean salinity stratification. Intense precipitation during the summer monsoon causes a large imbalance between precipitation (P), evaporation (E) and river runoff (R) in the BoB. The pool of freshwater at the surface forms a 'barrier' by enhancing the stratification of the water column (Vinayachandran et al. 2002). When a low saline water plume is present in the upper ocean, the mixed layer (region in upper ocean where density is homogeneous) is typically thinner than the isothermal layer (region in upper ocean where temperature is homogenous) and a BL is present (Sprintall and Tomczak 1992). Conversely when the mixed layer and isothermal layer have the same depth, no BL is present (see Figure 1.1). As such, the barrier layer thickness (BLT) is defined as the difference between the isothermal layer depth (ILD) and mixed layer depth (MLD). The presence of the BL acts to limit heat exchange within the water column, allowing the upper ocean to warm (Monetégut et al. 2007; Sengupta et al. 2008; Girishkumar et al. 2013), influencing the IOD (Qu and Meyers 2005; Qui et al. 2012), and tropical cyclone activity in the BoB (Balaguru et al. 2012). Knowing the location and magnitude of the BLT will help researchers and forecasters evaluate the evolution of these features more accurately.

The launch of National Aeronautics and Space Administration's (NASA) Aquarius Salinity/SAC-D and European Space Agencies (ESA) Soil Moisture Ocean Salinity (SMOS) missions has allowed for global sea surface salinity (SSS) measurements to be made on spatial and temporal scales that were previously impossible. Both of the satellites' onboard passive microwave radiometers measure sea surface brightness temperature using the L-band (1400-1427 MHz) frequency that is then converted to

salinity using a geophysical model. Both satellites have already been able to reveal the SSS structures of many phenomena. Being able to track the BL in near-real time using satellite observations is important for understanding upper ocean dynamics.

This thesis is divided into two research publications that examine oceanic and atmospheric processes in the Indian Ocean. These chapters are connected to the introduction (Chapter 1) and conclusions (Chapter 4).

Chapter 2 investigates the environmental alterations caused by ENSO over the BoB and how they influence tropical cyclone activity. Using National Center for Environmental Prediction-Department of Energy Global Reanalysis 2 (NCEP-DOE R-2 or NCEP-2) and Simple Ocean Data Assimilation (SODA) reanalysis, atmospheric and oceanic conditions during the altering phases of ENSO are investigated. An explanation for the observed increase in tropical cyclone activity during La Niña as compared to El Niño is presented and discussed.

Chapter 3 develops a method for estimating the BLT in the Indian Ocean using satellite observations. This study makes use of satellite derived SST, SSS, and SSHA as well as Argo temperature and salinity profiles, and HYbrid Coordinate Ocean Model (HYCOM) simulations. The connection between each remotely sensed parameter and the BL are assessed and described. A multilinear regression model (MRM) is then developed to estimate the barrier layer from the remotely sensed variables. A comparison between MRM BLT values with Argo and HYCOM shows that remotely sensed SSS can be used to track the barrier layer in the Indian Ocean. A final conclusion section (Chapter 4) summarizes the overall findings of both works and develops directions for future work.

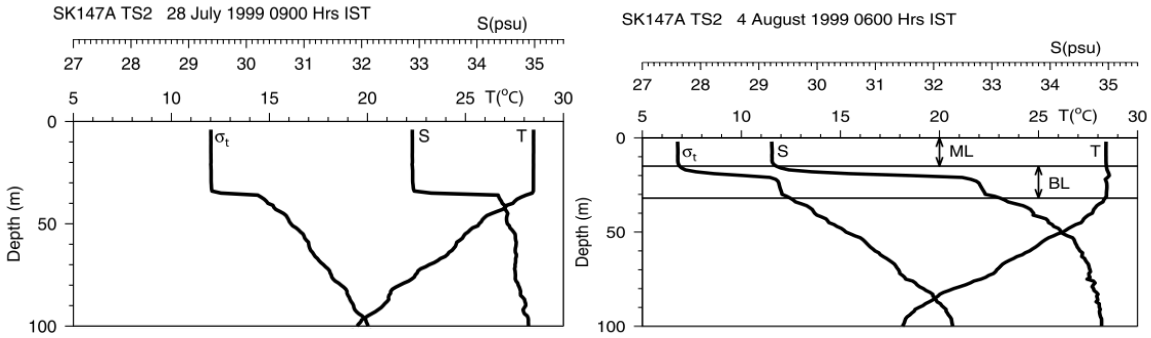

Figure 1.1: Vertical profiles of temperature (T), salinity (S) and density (σ_t) in the upper 100-m of the water column (left) in the absence of a low saline water plume and (right) in the presence of a low saline water plume with a barrier layer (BL) present. These profiles are from the Bay of Bengal (Source: Vinayachandran et al. 2002).

CHAPTER 2

ENSO-MODULATED CYCLOGENESIS OVER THE BAY OF BENGAL[1]

[1]Felton, C. S., B. Subrahmanyam, and V. S. N. Murty, 2013: ENSO-Modulated Cyclogenesis over the Bay of Bengal. *J. Climate*, **26**, 9806–9818. doi: 10.1175/JCLI-D-13-00134.1

ABSTRACT

The role of El Niño Southern Oscillation (ENSO) on the modulation of tropical cyclone activity over the Bay of Bengal (BoB) for the 1979-2011 period is examined. It is shown that Niño3.4 sea surface temperature (SST) anomalies are negatively correlated with the BoB tropical cyclone activity to a statistically significant percentage by a lead-time of five months. Composites of 10-meter zonal winds exhibit greater variance during La Niña events favoring the development of low-level cyclonic vorticity. Low vertical wind shear over the central and northern BoB also aids the development of tropical cyclones during La Niña events. Increased relative humidity is the result of enhanced moisture transport and higher precipitable water under La Niña conditions. Furthermore, storm relative composites of relative humidity show stronger moisture pulses over the BoB during La Niña. The enhanced moisture associated with tropical cyclogenesis likely aids the development and strengthening of the systems. ENSO forces modulations in oceanic conditions as well. The observed negative (positive) SST anomalies during La Niña (El Niño) could be seen as the result of increased (decreased) net heat flux across the sea surface. Tropical cyclone activity varies between El Niño and La Niña due to anomalous wind and moisture patterns during each ENSO phase.

2.1. INTRODUCTION

Tropical cyclones (TCs) are among the most destructive natural events that form in the world's oceans. Characterized by strong winds, heavy rainfall, and destructive storm surge, TCs cause considerable economic and societal damage along coastlines as well as further inland. The Bay of Bengal (BoB) is one of the more vulnerable regions to these effects due to its low-lying topography and population density along the coastline. The BoB is a semi-enclosed ocean-basin, located in the Northern Indian Ocean that exhibits a unique bimodal seasonal distribution of tropical cyclone activity (Fig. 2.1) due to unfavorable environmental conditions during the monsoon season (Z. Li et al. 2013). Peak TC activity occurs during October-December (post-monsoon) with a secondary maximum during March-May (pre-monsoon). In order to forecast TCs accurately, it is necessary to understand the environmental factors that influence TCs in this region.

Oceanic and atmospheric conditions are important for the development, strengthening and movement (track) of tropical cyclones across the BoB. The seasonal and intraseasonal transitions play an important role in altering TC environment in the BoB (Goswami et al. 2003; Kikuchi and Wang 2010; Yanase et al. 2012). Recent studies (Kikuchi et al. 2009; Lin et al. 2009; McPhaden et al. 2009; Maneesha et al. 2012) have highlighted the importance of oceanic thermal structure on the intensification of very severe cyclonic storm Nargis that devastated Myanmar in 2008. The study by Singh et al. (2000) has shown that tropical cyclone (TC) activity during the seasonal peaks of November and May is trending upwards and exhibits a prominent El Niño-Southern Oscillation (ENSO)-scale oscillation of 2-5 years over the BoB.

The ENSO is well known to be one of the primary climatic features causing global alterations in atmospheric and oceanic patterns. The two extremes associated with the ENSO, termed as El Niño and La Niña events, describe the SST anomalies (SSTAs) in the central Pacific Ocean (Bjerknes, 1969). The ENSO signal exhibits similar seasonal progressions, with SSTAs beginning to emerge in the central Pacific Ocean during April-June, peaking later during November-January. Though research on the affect of the ENSO on tropical cyclones in the Atlantic and Pacific Oceans is well documented, far less research has been conducted over the BoB. Alterations in SST and relative vorticity during El Niño facilitate increased cyclogenesis during July-August of El Niño years in the BoB (Singh et al. 2001). Camargo et al. (2007) found that vertical wind shear played the primary role in altering tropical cyclogenesis locations in the BoB during ENSO events after examining the parameters that compose a genesis potential index developed by Emanuel and Nolan (2004). Recent research by Girishkumar and Ravichandran (2012) (from here onwards GR (2012)) indicates that ENSO influences tropical cyclone environment over the BoB during October-December by forcing anomalous patterns in convection, low-level cyclonic vorticity, and tropical cyclone heat potential (TCHP). The present study looks beyond these findings by investigating the large-scale dynamics forcing these and other important environmental modulations.

Research on the impacts of the ENSO on tropical cyclones over the BoB is limited compared to other ocean basins. In this paper, we focus on the period from 1979-2011 to investigate the ENSO forced modulations in environmental conditions over the BoB. In addition, we diagnose the impacts on tropical cyclone activity. This paper is organized as follows: Section 2 describes the data set and methods used for the study. An overview of

TC activity over the BoB during ENSO events is presented in section 3. Section 4 investigates the impact of the ENSO on TC environment in the BoB. A summary and discussion of the findings are presented in section 5.

2.2. DATA AND METHODS

Northern Indian Ocean TC tracks are obtained from the U.S. Navy's Joint Typhoon Warning Center's (JTWC) best track data site (http://www.usno.navy.mil/JTWC/). The best track data is filtered to remove storms that 1) formed over the Arabian Sea, 2) formed over land, and 3) did not track into the BoB. The remaining storms that reached minimum wind speeds of 20 knots (kt) are only included. For this study tropical cyclogenesis (depression formation) occurs at this minimum value (20 kt) since the JTWC records maximum wind observations at 5 kt increments with most storms being identified when a minimum wind speed of 20 kt was achieved. While the India Meteorological Department (IMD) defines a tropical cyclone when the wind speeds exceed 34 kt, the JTWC database utilizes 35 kt. For this reason wind speeds $\geq$ 35 kt are used as the threshold value for tropical cyclones while 20 - 34 kt is used for depressions throughout the analysis.

Monthly average SST data for the Niño3.4 region (5°N-5°S, 120°W-170°W) is obtained from the National Oceanic and Atmospheric Administration's (NOAA) Climatic Prediction Center (http://www.cpc.ncep.noaa.gov/) for the 1979-2011 period in order to calculate the Niño3.4 index for the study. Seasons are termed as "El Niño" or "La Niña" if the 5-month running mean SSTAs exceed a threshold value of ±0.4°C for 6 months or more consecutive months as defined by Trenberth (1997).

Daily and monthly atmospheric analysis estimates (wind and relative humidity) from the National Center for Environmental Prediction Department of Energy Intercomparison Model Project reanalysis 2 (NCEP-DOE R-2 or NCEP-2) for the period 1979-2011 are used in this study. The horizontal resolution of the product is 2.5° x 2.5° grid with 17 levels in the vertical (Kanamitsu et al., 2002). Composites are created for El Niño and La Niña events during the post-monsoon season using the NCEP-2 data. A storm relative reference frame is adopted to examine the variability of atmospheric parameters before, during and after the formation of tropical systems. In order to remove the possible influence of the tropical cyclone on the spatial fields, daily estimates are smoothed following similar methods as in Kurihara et al. (1990). This method removes all wavelengths less than 7.5°. To reduce the possible impact of a tropical cyclone on the temporal fields, a 15-day filter is also applied. 10-meter wind estimates are linearly interpolated onto a 2° x 2° grid from the original Gaussian grid in order to perform the filtering method. Comparisons between high-pass filtered and smoothed linearly interpolated 10-meter wind estimates yielded similar results. All atmospheric anomalies are based off of the 33-year October through December means (1979-2011).

Vertically integrated moisture transport (**Q**) and precipitable water (W) are used to diagnose moisture content over the BoB during ENSO events. If the atmosphere is assumed to be in hydrostatic balance, p can be expressed as a vertical coordinate. Precipitable water (W, kg m^{-2}) in the air column can then be expressed by

$$W = g^{-1} \int_{ps}^{pt} q dp, \tag{1}$$

where g is the acceleration due to gravity (9.81 m s^{-2}), q is the specific humidity (kg kg^{-1}), *ps* is pressure at the surface (Pa) and *pt* the pressure at the top of the atmosphere (Pa). The total moisture transport **Q** (kg m^{-1} s^{-1}) above the Earth's surface can be written as

$$\mathbf{Q} = g^{-1} \int_{ps}^{pt} q\mathbf{V} dp, \tag{2}$$

where **V** represents the total wind vector (m s^{-1}), u (positive eastward) and v (positive northward). Vertical integrations were preformed using the trapezoidal rule from lowest model level, *ps* (1000 hPa), to the highest level where humidity is available, *pt* (300 hPa). Mixing ratio is computed from vertical profiles of temperature and relative humidity from the NCEP-2 reanalysis following methods from Bolton (1980).

Monthly outgoing long wave radiation (OLR) and Global Precipitation Climate Project (GPCP) precipitation data are used as proxies for vertical motion and convective activity during each ENSO regime. The NOAA/OAR/ESRL PSD, Boulder, Colorado, USA provided both datasets from their web site at http://www.esrl.noaa.gov/psd/. Each product has a horizontal resolution of 2.5° x 2.5°.

Simple Ocean Data Assimilation (SODA) reanalysis data is used to discern the sea surface temperatures patterns (SST) during each respective ENSO phase. In this study, we used SODA version 2.2.4 reanalysis output from 1979-2008 (Giese and Ray, 2011). Anomalies are based off the October through December means from 1979-2008. This version of SODA combines an ocean model based on the Parallel Ocean Program (POP) version 2.0.1 numerics (Smith et al., 1992) with the assimilation of hydrographic temperature and salinity data. The model outputs are mapped onto a uniform 0.5° × 0.5° horizontal grid with 40 levels in the vertical. The use of data assimilation allows sparse

observational datasets to be optimally merged with high performance ocean models to provide an estimation of ocean variables.

2.3. CLIMATOLOGY OF TROPICAL CYCLONES DURING ENSO

a. Seasonal Tropical Cyclone Activity

Before examining the impact of the ENSO on tropical cyclone environment, a brief climatology of TC activity over the BoB is presented. In order to take into account the strength, number and duration of the tropical cyclones for analysis, accumulated cyclone energy (ACE) is calculated using the formula (3):

$$ACE = 10^{-4} \sum v_{\max}^2, \tag{3}$$

where v_{max} is the sustained maximum wind speed in knots from the 6-hourly JTWC observations. The values are summed over the life of each tropical system when wind speeds are in excess of 35 knots. Seasonal tropical cyclone occurrences and ACE for each month over the study period (1979-2011) are shown in Fig 2.1. Two seasonal peaks can be seen in May and October when atmospheric and oceanic conditions are most favorable over the BoB (Z. Li et al. 2013). During the period from 1979-2011, a total of 118 tropical systems formed over the BoB with 74 occurring from October through December (post-monsoon) and 25 from March through May (pre-monsoon). Of the 74 storms that formed during the post-monsoon season, 31 developed during La Niña events while only 16 occurred during El Niño events (Table 2.1). Comparing only developing depressions (i.e. TCs with maximum speeds > 35 kt), TCs during La Niña are twice as prevalent when compared to El Niño years. The post-monsoon tropical cyclone genesis locations and tracks during El Niño (Fig 2.2a) and La Niña (Fig 2.2b) events also show differing

trends. Genesis locations and tracks during El Niño events trend more westward (85.2°E) while during La Niña years there is a significant (p <0.01, t test) eastward (90.6°E) shift in genesis sites with wider varying track and landfall patterns. Pre-monsoon TC genesis and tracks are shown in Fig 2.3. Tracks are not separated by ENSO phase due to the low number of ENSO events (2 El Niño, 4 La Niña respectively) extending into the pre-monsoon season. Landfalls are concentrated along the northern and western BoB due to the prevailing upper wind patterns prior to the monsoon season.

b. Post-monsoon TC Activity

To determine the connection between ENSO and TC activity over the BoB, a series of statistical analyses are performed. Correlation tests between October–December averaged ACE and monthly Niño3.4 SSTA can be seen in Table 2.2. Correlations during all months were negative with the highest and most significant occurring from May (-0.38, $p < 0.05$) increasing until December (-0.66, $p < 0.01$). These results agree with the findings of GR (2012) that ACE is negatively correlated during October – December and that tropical cyclone activity during La Niña (El Niño) years is higher (lower). Increasing correlations found from May to December are the result of the lead-lag relationship between ENSO and TC activity over the BoB. The development of an ENSO event typically leads post-monsoon TC activity, which explains why correlations increase towards the start of the post-monsoon TC season. These results show that the boreal summer Niño3.4 SSTAs are significantly correlated with ACE during the post-monsoon season indicating that the Niño3.4 index can serve as a proxy for TC activity in the months prior to a mature ENSO event.

c. Pre-monsoon TC Activity

Due to the seasonal locking of ENSO, events typically do not persist into the pre-monsoon tropical cyclone season over the BoB. However, these months represent a time when ENSO events have ceased a few months prior or may commence in the upcoming months. To test if a lagged or preceding ENSO signal is present, correlations are run between the Niño3.4 SSTAs and ACE from March to May (Table 2.3). Correlations were low and all relationships failed to reach statistically significant values indicating that an ENSO signal is not present in March – May ACE totals. Correlations are poor during this time since the ENSO typically peaks around December and the signal weakens from March through May when the northward-propagating intraseasonal oscillations dominate the environment over the BoB (K. Li et al. 2013). Since the correlations between ACE and Niño3.4 SSTAs during the pre-monsoon season are poor, the rest of the paper will focus on the post-monsoon time frame.

2.4. MODULATION OF BOB ENVIRONMENT DURING ENSO

To determine the ENSO forced modulations over the BoB, an analysis of the environmental factors that contribute to convection and tropical cyclones is performed. Relative humidity, vorticity, wind shear and SSTs have been shown to be the major environmental parameters that impact seasonal tropical cyclone formation over the BoB (Singh et al. 2001; Kikuchi and Wang 2010; Yu and McPhaden 2011; Yanase et al. 2012). As such, our analyses focus on these parameters. Low-level winds are important for TC development since they can transport moisture and enhance cyclonic vorticity. The low-level jet over the Indo-Chinese peninsula is weaker El Niño (Fig. 2.4a) while during La Niña, the jet is stronger leading to enhanced convergence (Fig. 2.4b). Wind

anomalies reverse direction along the southern BoB between ENSO phases due variations in convective activity, which will be examined later. This results in anomalous anti-cyclonic vorticity over the central and western BoB during El Niño events (Fig. 2.4c) and anomalous cyclonic vorticity during La Niña (Fig. 2.4d). The increase in low-level cyclonic vorticity favors TC development during La Niña comparatively.

Large-scale wind patterns force ascent over the BoB during La Niña events as well. OLR (Fig. 2.5a) and GPCP (Fig. 2.5b) anomalies indicate ENSO altered convective and precipitation patterns due to the ENSO. During El Niño, convective activity over the eastern BoB and Gulf of Thailand is reduced (Fig. 2.5a). Convection in this region is typically sustained by the heat and moisture fluxes from high SSTs and the rising limb of the Walker Cell. During El Niño, the rising limb of the Walker Cell, and associated convection, moves eastward in response to enhanced SSTs over the Central Pacific. The presence of positive OLR and negative precipitation anomalies indicate that sinking motion is enhanced during El Niño events due to this eastward shift. Conversely, the patterns during La Niña are reversed. Lower OLR values (enhanced convection) and higher precipitation are present over the eastern BoB and Indo-Chinese peninsula are due to the enhancement of the Walker cell's rising limb over the western Pacific and Indonesia (Fig. 2.5b). The increase in convective activity and precipitation act to precondition the atmosphere for tropical cyclone development through enhanced moisture and lift.

Westerly winds along the equator south of the BoB are also important for the generation of westerly wind bursts which generate enhanced cyclonic vorticity in the lower levels of the atmosphere (Kikuchi et al. 2009). The cyclonic rotation in the lower

levels acts to remove the low level stable air mass that forms below intense convection due to latent cooling from precipitation outflow (Gray 1998). This results in higher pressure in the lower level of the atmosphere that weakens convergence under the convective system. The presence of background cyclonic vorticity acts to remove the stable air mass and provide convergence for convective systems favoring development. Once the low level stable air is removed, air-sea fluxes can begin to initiate, leading to tropical cyclone development if environmental conditions are favorable. Over the BoB, zonal 10-m winds exhibit more variance during La Niña (Fig. 2.6). Surface winds in equatorial regions are largely driven by pressure differentials due to the weak Coriolis force. The presence of enhanced convective activity over the eastern BoB and Indian Ocean creates a favorable environment for these wind bursts to occur by mass conservation arguments. As the post-monsoon season progresses surface winds begin to blow from the northeast. With the presence of strong westerly winds along the equator this creates low-level cyclonic flow. Furthermore, winds over Thailand and the Malay Peninsula also exhibit more variance, favoring the development of low-level cyclonic flow. Stronger surface winds can also facilitate moisture flux into the atmosphere, which will be examined later.

Wind shear is another important environmental parameter that impacts tropical cyclogenesis (Gray, 1968). The highest environmental wind shear during TC genesis for all storms over the study period was 26 m s^{-1}. Climatological wind shear over the entire BoB remains below this value under both El Niño and La Niña regimes. Both ENSO phases exhibit wind shear minima over the central BoB where tropical cyclones form, similar to climatological conditions (Fig. 2.7a). However, shear anomalies reverse sign

over the northern and southern BoB between El Niño (Fig. 2.7b) and La Niña (Fig. 2.7c). Yanase et al. (2012) have shown that shear increases over the southern BoB in the days prior to tropical cyclogenesis indicating that higher shear found during La Niña is favorable for TC development. The enhanced shear during La Niña can act to strengthen convective systems through the tilting and stretching of horizontal vorticity. In the presence of non-uniform rising vertical motion, such as a convective system, and background horizontal vorticity, the horizontal vorticity can be tilted unevenly resulting in the vertical vorticity. This induces additional rising motion stretching the vortex and increases vorticity further. As these systems track into the central BoB where vertical shear is lower, tropical cyclone development can occur. This is limited during El Niño due to the presence of higher shear in the northern BoB. The anomalous wind shear patterns are due to ENSO altered meridional temperature profiles (not shown). During El Niño, temperatures are cooler near the top of the atmosphere at 20°N/S. This enhances the meridional temperature gradient and strengthens wind shear over the northern BoB by thermal wind arguments. The pattern is reversed during La Niña. Temperatures are warmer and the weakened meridional temperature gradient causes wind shear to weaken over the northern BoB. This favors the development of tropical systems that track into the northern BoB and explains why more TC formation is favored during La Niña.

Previous research on the role of vertical wind shear over the BoB during the ENSO has yielded conflicting results. Camargo et al. (2007) determined that wind shear was the limiting parameter while GR (2012) noted that shear had a negligible impact on TC formation. Due to the short time scale of TCs, the climatological analysis by the previous authors may not be capturing the variability of wind shear that drives the difference in TC

activity between ENSO phases. In order to investigate the impact of ENSO on daily wind shear, a storm relative reference frame is adopted. Shear is averaged zonally over the BoB ±30 days relative to storm formation from the equator to 25°N. The anomalies are determined from the background mean shear (33-year) centered on the mean genesis date (day 314). Both regimes exhibit different patterns prior to genesis (Fig. 2.8). During La Niña shear increases along the entire southern BoB in the days prior to genesis (Fig. 2.8b). An examination of the 200 hPa and 850 hPa winds indicates that the increase in shear is primarily due to strengthened 850 hPa zonal winds (not shown). The significantly weaker shear over the northern BoB favors the development and strengthening of TCs as they track northwards. Additionally, the increase in low-level zonal winds provides additional background low-level vorticity for cyclones to develop. The pattern during El Niño is significantly different with weaker shear over the southern BoB (Fig 2.8a). The decrease in wind shear over the equatorial region is less favorable for cyclones to form because of less background cyclonic vorticity. Examining the environment around each storm during El Niño, conditions are similar to the background mean with weak anomalies. This indicates that shear is decreasing, relative to Fig. 2.7a, over the northern BoB prior to genesis allowing for TCs to develop. The number of days when shear is greater than 20 m s^{-1} also varies significantly between La Niña (9.1 days) and El Niño (2.6 days) phases ($p < 0.05$, t test). Positive shear anomalies over the southern BoB serve as a proxy for cyclonic low-level vorticity, which is more conducive for TC formation during La Niña.

Mid-level humidity also plays an important role in the development of tropical systems. Anomalous positive relative humidity pulses have been linked to TC

development during October and November over the BoB (Yanase et al. 2012). Z. Li et al. (2013) showed that higher relative humidity from October to November favors more tropical cyclogenesis during these months in comparison to the April to May when relative humidity is lower. Humidity is higher over the BoB at both the 700 hPa (Fig. 2.9a) and 850 hPa (Fig 2.9b.), leading to favorable conditions for enhanced cyclogenesis during La Niña events. To determine the cause of the comparatively higher humidity values during La Niña, vertically integrated moisture transport and precipitable water are examined (Fig. 2.10). Climatological integrated moisture transport and precipitable water favor high moisture content over the entire southern BoB (Fig. 2.10a,b). Wind patterns during El Niño (Fig. 2.10c) result in weaker moisture transport over the BoB. The weakened jet over the Indo-Chinese peninsula and stronger easterlies along the equator lead to less precipitable water over the BoB (Fig. 2.10d). Conversely under the La Niña regime (Fig. 2.10e), westerly winds along the equator and southern BoB transport moisture towards the region. This results in the accumulation of precipitable water (Fig. 2.10f) over the central and eastern BoB. The additional moisture during La Niña supports enhanced convection and precipitation, shown in Fig. 2.4, which are important environmental conditions for cyclogenesis to occur. Enhanced moisture also favors latent heat release that is required for TC development and strengthening.

Large absolute vorticity and high relative humidity variability with a periodicity of approximately 30 to 40 days has been linked to tropical cyclone formation over the BoB (Yanase et al. 2012). To further diagnose the impact of relative humidity, a storm relative reference frame is adopted (as in Fig. 2.8). Patterns during each ENSO phase exhibit distinct evolutions in time (Fig. 2.11). Enhanced moisture over the southern BoB occurs

during both El Niño event (Fig. 2.11a) and La Niña events (Fig. 2.11b) 20 to 30 days before genesis. Anomalously dry air is present over the northern BoB in the El Niño composite that is much weaker during La Niña. The presence of drier air over the northern BoB inhibits TC formation during El Niño, while during La Niña, TC activity is distributed over the entire BoB due to comparatively more moisture. These results are consistent with those of Yanase et al. (2012) that TC formation coincides with a northward propagating humidity pulse. The new finding is that a humidity signal appears in both ENSO phases, but TC genesis is favored during La Niña due to enhanced moisture over the entire BoB. This signal could be the result of ENSO altered Madden-Julian Oscillations and should be examined in the future.

Sea surface temperatures (SSTs) have been shown to play a crucial role in the development and strengthening of tropical systems in the BoB (Singh et al. 2001; Yu and McPhaden 2011). SODA SSTAs exhibit differing patterns during El Niño (Fig. 2.12a) and La Niña (Fig. 2.12b). Under La Niña conditions, anomalously strong winds force evaporation that cools SSTs, while during El Niño weaker winds allow for SSTs to rise in the southern BoB. The anomalous OLR fields also contribute to the observed temperature differences. Warming or cooling during each ENSO phase in the Indian Ocean is primarily attributed to basin wide surface heat flux anomalies (Hong et al. 2010). Increased wind variability creates a positive feedback cycle between surface winds and convection with enhanced evaporation supporting enhanced atmospheric convection resulting in cooler SSTs. Enhanced (inhibited) convective activity forced by La Niña (El Niño) blocks (allows) solar radiation to reach the ocean surface resulting in cooling (warming) over the northern BoB. The drop in SSTs is small during La Niña due to

enhanced stratification in the upper ocean (Murty et al. 1996, Bhat et al. 2002, Vinayachandran et al. 2002, Sengupta et al. 2008). SSTs are above 28°C during both regimes, well above the tropical cyclone formation threshold value of 26.5°C, and support the findings by GR (2012). Future research will be directed towards determining the exact cause of the differences between SSTAs between ENSO events over the BoB.

2.5. SUMMARY AND DISCUSSION

Post-monsoon season tropical cyclone activity is more favorable during La Niña events over the BoB due to a variety of factors. Previous studies have shown that Niño3.4 SSTAs are correlated with ACE during the post-monsoon season (GR, 2012). We have shown through statistical analyses that La Niña events are correlated with an increase in tropical cyclone activity (ACE) in the BoB at extended lead times (up to 5 months) during the post-monsoon season. This indicates that Niño3.4 SSTAs can be used as a predictor for the upcoming post-monsoon tropical cyclone seasons. An analysis performed for the pre-monsoon season shows no statistical relationship between ACE and Niño3.4 SSTAs over the time period of the study.

Previous research by Camargo et al. (2007) examines TC activity conditions impacted by ENSO globally using Emanuel and Nolan's (2004) Genesis Potential Index (GPI). The analysis was conducted on environmental parameters averaged over a three-month time frame, which coincided with the months prior to peak TC activity over the BoB (August – October). In this study we examined the climatological patterns and daily evolution of the parameters known to impact TC formation during the peak season over the BoB (October – December). The results of Camargo et al. (2007) concluded that lower shear over the BoB during August – October was driving the differences in observed TC

activity. Our results show the increase in shear over the equator and decrease over the northern BoB play an important role on modulating TC genesis and intensity during La Niña.

GR (2012) pointed out the important connection between tropical cyclone activity and the ENSO signal and analyzed some environmental conditions. We expand upon these findings and show that the ENSO signal also leads TC activity over the BoB by a period of 5-6 months. The findings of GR (2012) also contradict those of Camargo et al. (2007) concluding that climatological wind shear patterns were similar during both ENSO phases and did not play an important role in modulating TC activity. Our analyses reveal that the increase (decrease) in shear over the southern (northern) BoB during La Niña favors TC development. GR (2012) also did not examine humidity patterns during the ENSO and this is elaborated in this study. We also work through the synoptic conditions that led to the ENSO altered wind patterns observed over the BoB.

Composites of low-level winds constructed over the BoB for the post-monsoon season (October – December) show cyclonic (anticyclonic) patterns during La Niña (El Niño). This anomalous vorticity is caused by anomalous westerly (easterly) winds that arise as a result of enhanced (suppressed) convective activity over the eastern BoB and Indian Ocean. The large-scale cyclonic rotation provides a favorable environment by supplying additional background vorticity for TC formation. Convective conditions observed during La Niña also create a suitable synoptic pattern for wind bursts to occur due to the increase zonal 10-m wind variance. These wind bursts are important since they help generate low-level cyclonic vorticity, aiding TC development.

La Niña events have enhanced cyclonic vorticity due to favorable atmospheric circulation patterns. During both ENSO phases, climatological vertical wind shear was below 26 m s^{-1}, the maximum wind shear during TC genesis. Higher shear over the equatorial and southern BoB aids the development of convective systems during La Niña events. As convective complexes track into the low shear environment in the central BoB TC formation is favored. Relative humidity is also higher over the BoB during La Niña events due to the environmental wind patterns that favor high precipitable water patterns. An examination of humidity patterns leading up to TC formation shows a stronger northward propagating signal during La Niña that favors TC formation. Patterns during El Niño limit the northward progression of the humid air mass due to drier air over the northern BoB that restricts TC development. Future research should investigate if this signal is associated with ENSO altered Madden-Julian Oscillation patterns since the periodicity of the humidity signal is within the MJO band (~30 days). SST cooling is the result of increased latent heat flux due to stronger winds and increased cloud cover due to convective activity during La Niña. The cooler SSTs serve as a proxy for increased evaporation aiding convective activity and increasing precipitation seen in the OLR and GPCP composites. Wind patterns favor moisture accumulation over the BoB, which supports the observed enhanced convection during La Niña.

The variation in tropical cyclone activity over the BoB during ENSO events is forced by a combination of factors. La Niña conditions comparatively offer a more favorable environment due to low-level cyclonic vorticity, wind patterns, and increased moisture.

Table 2.1: Occurrences and frequencies of the tropical systems (cyclones and depressions) during the post-monsoon season (October – December) over the Bay of Bengal for ENSO events. The number of tropical systems that comprise the total and did not reach a minimum wind speed of 35 knots during its lifetime are shown in parentheses.

ENSO Cycle	Number of Years	Number of Tropical Systems	Tropical Systems per Year
El Niño	10	16 (2)	1.60
Neutral	12	27 (6)	2.25
La Niña	11	31	2.82

Table 2.2: Correlation coefficients between monthly Niño3.4 SSTAs and ACE totals from October – December (1979-2011). Italicized (bolded) values signify correlations where *p*-values < 0.05 (0.01).

Month	Correlation Coefficients
Jan	-0.02
Feb	-0.05
Mar	-0.11
Apr	-0.24
May	*-0.38*
Jun	**-0.50**
Jul	**-0.56**
Aug	**-0.58**
Sep	**-0.60**
Oct	**-0.62**
Nov	**-0.64**
Dec	**-0.66**

Table 2.3: Same as Table 2.2, except for the months of March through May (1979-2011). Negative values (-1) next to month names indicate Niño3.4 SSTAs taken from the previous year while zeros (0) are from the concurrent year of the ACE totals. No correlations have *p*-values < 0.05.

Month	Correlation Coefficients
Jun (-1)	-0.12
Jul (-1)	-0.08
Aug (-1)	-0.06
Sep (-1)	-0.06
Oct (-1)	-0.07
Nov (-1)	-0.07
Dec (-1)	-0.06
Jan (0)	-0.05
Feb (0)	-0.03
Mar (0)	0.00
Apr (0)	0.09
May (0)	0.21

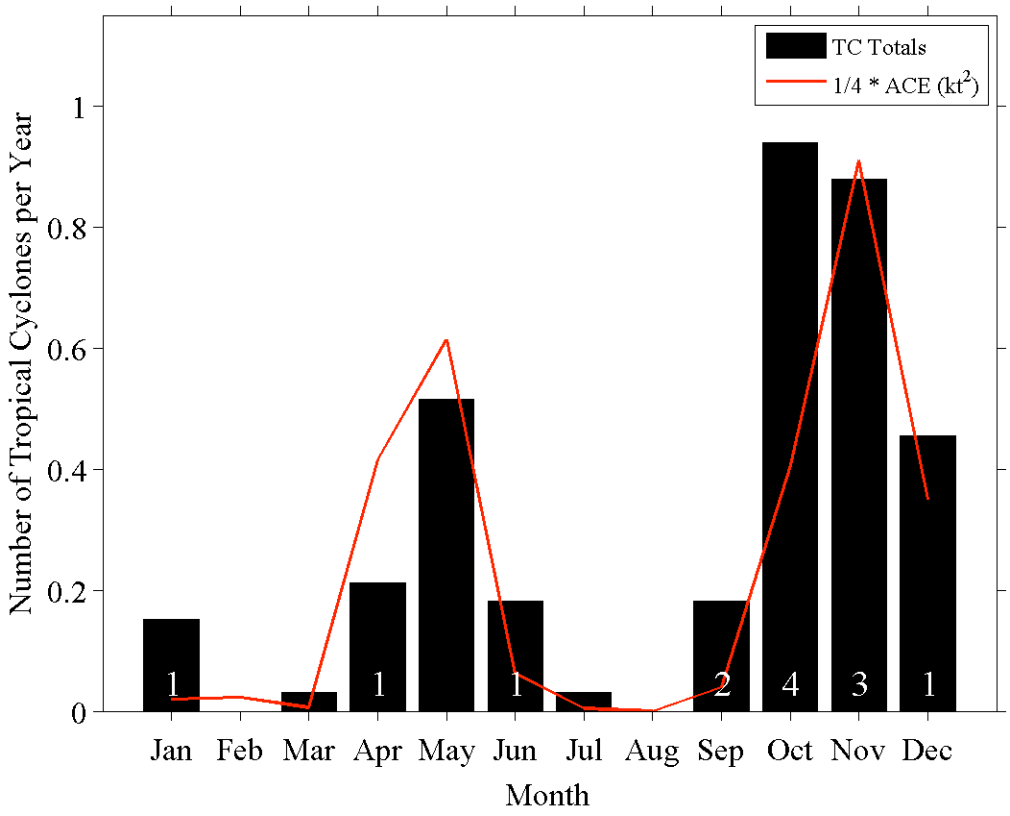

Figure 2.1: Seasonal distribution of tropical systems and ACE (kt^2) in the Bay of Bengal over the study period of 1979-2011. ACE is scaled by a factor of ¼ for ease of comparison. The white numbers in each column represent the number of tropical systems that formed during each month without attaining the threshold value of 35 knots during its lifetime over the 33-year time period.

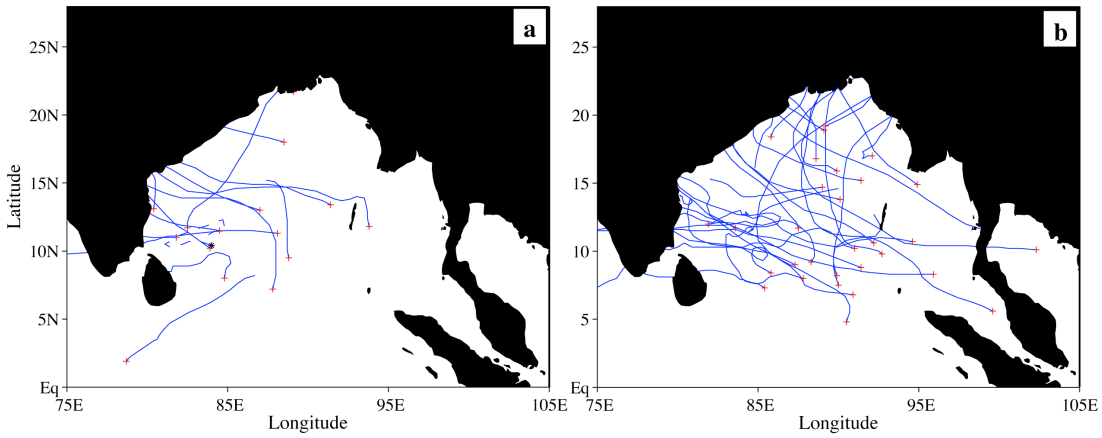

Figure 2.2: Post-monsoon season (October- December) tropical cyclone genesis and tracks during (a) El Niño and (b) La Niña events over the period of 1979-2011 in the Bay of Bengal. Red plus signs (blue solid lines) indicate genesis locations (track) for storms that reached a minimum wind speed of 35 knots over its lifetime. Black stars (dashed blue lines) indicate genesis locations (tracks) for storms that did not reach a minimum speed of 35 knots.

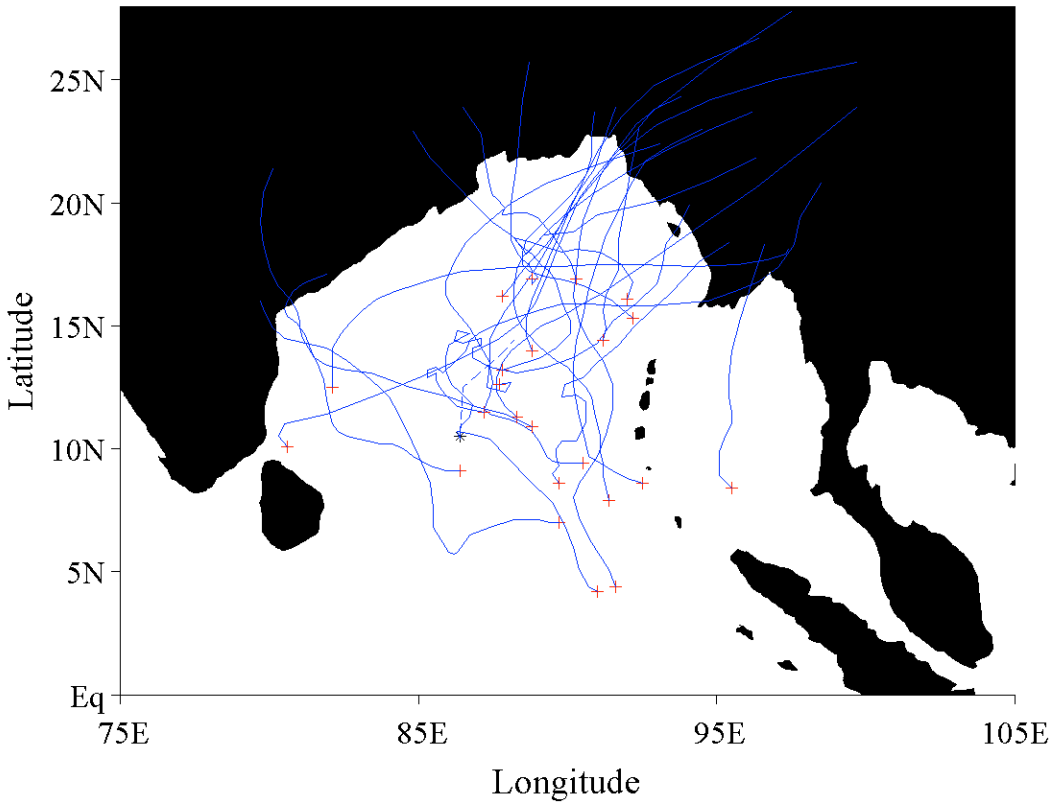

Figure 2.3: Pre-monsoon season (March - May) tropical cyclone genesis locations and tracks in the Bay of Bengal over the period of 1979-2011. Red plus signs (blue solid lines) indicate genesis locations (track) for storms that reached a minimum wind speed of 35 knots over its lifetime. Black stars (dashed blue lines) indicate genesis locations (tracks) for storms that did not reach a minimum speed of 35 knots.

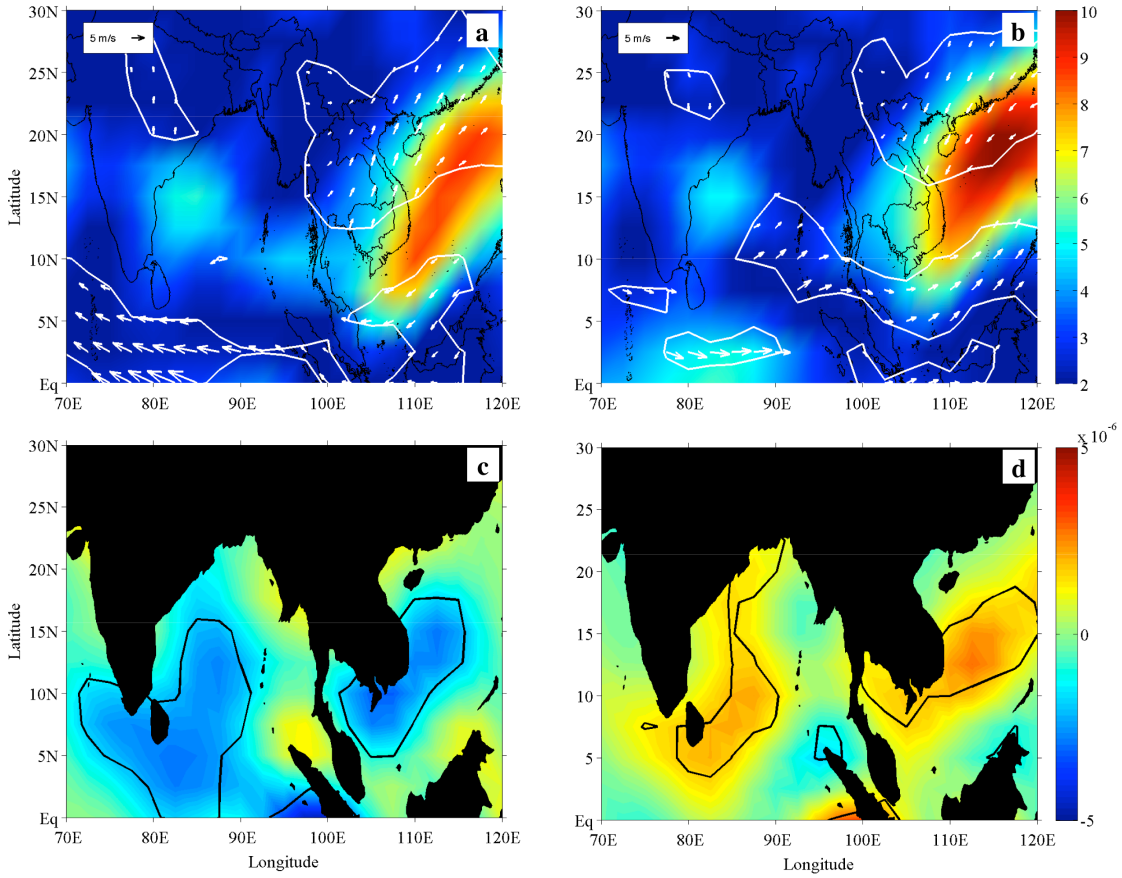

Figure 2.4: (Top Shaded) Post-monsoon season (October-December) averaged 925 hPa wind magnitude (m s^{-1}) composites during (a) El Niño events and (b) La Niña events. (Top) Vectors represent wind anomalies during each ENSO phase where $p < 0.1$ using a Student's t test relative to the 33-year mean. (Bottom) Same as top, but for 925 hPa relative vorticity anomalies (s^{-1}) during (c) El Niño events and (d) La Niña events. Positive (negative) values correspond to anomalous cyclonic (anti-cyclonic) vorticity.

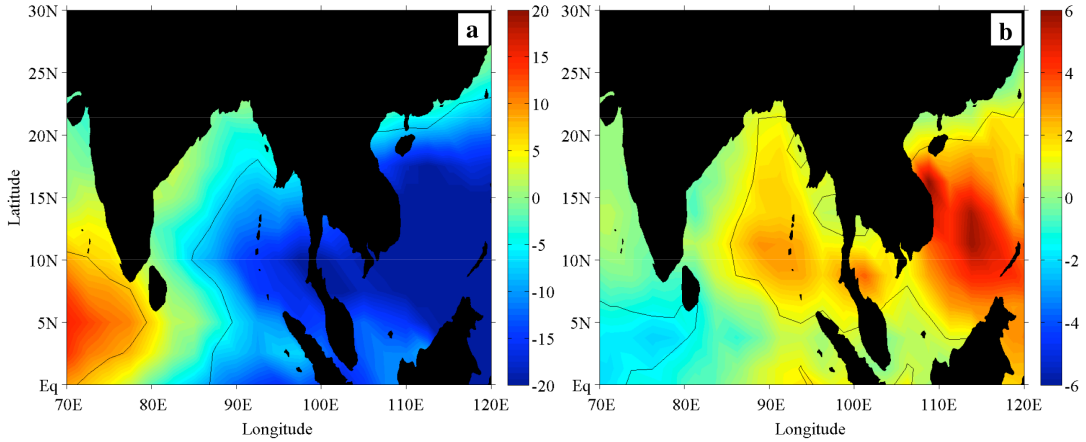

Figure 2.5: Difference in post-monsoon season (a) OLR (W m^{-2}) and (b) GPCP precipitation anomalies (mm day^{-1}) between La Niña and El Niño. Regions enclosed by contouring represent differences in the anomalies between El Niño and La Niña at $p < 0.1$ using a Student's *t* test. Negative OLR values correspond indicate stronger convection during La Niña while positive precipitation values indicate higher precipitation during La Niña events.

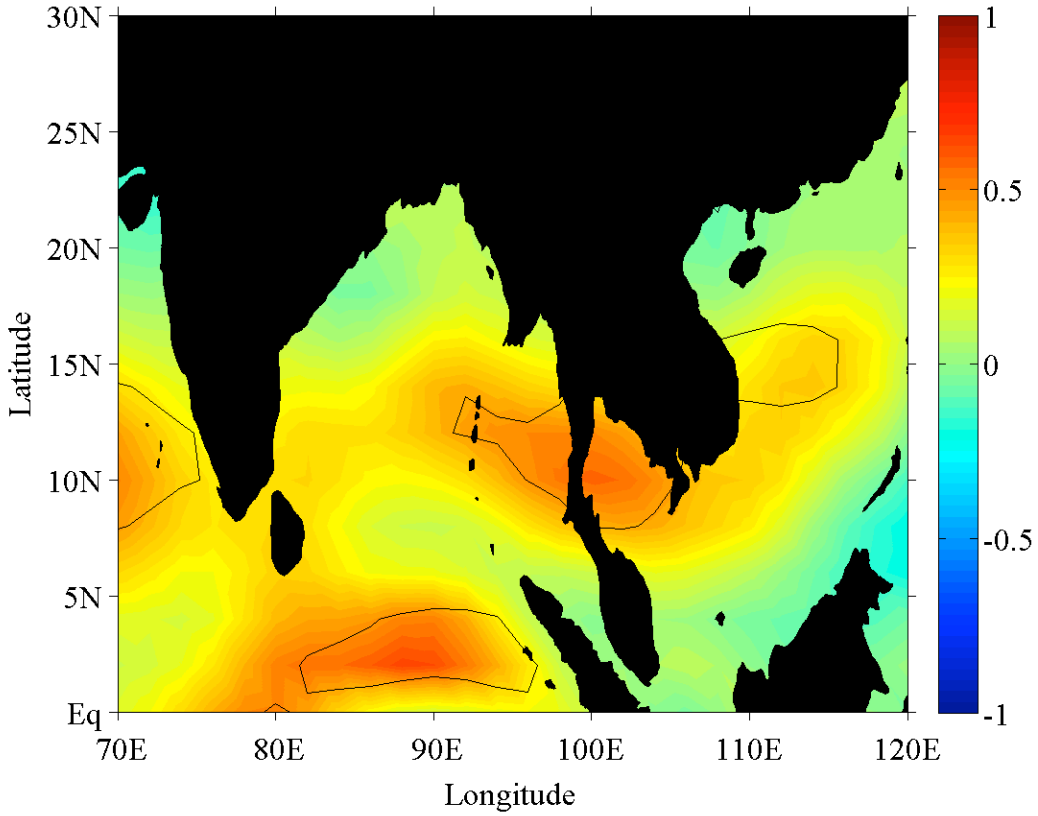

Figure 2.6: Difference of 10-meter zonal wind standard deviation between La Niña and El Niño. Regions enclosed by contouring represent differences in the anomalies between each El Niño and La Niña at $p < 0.1$ using a Student's t test. Positive (negative) values indicate greater variance during La Niña (El Niño).

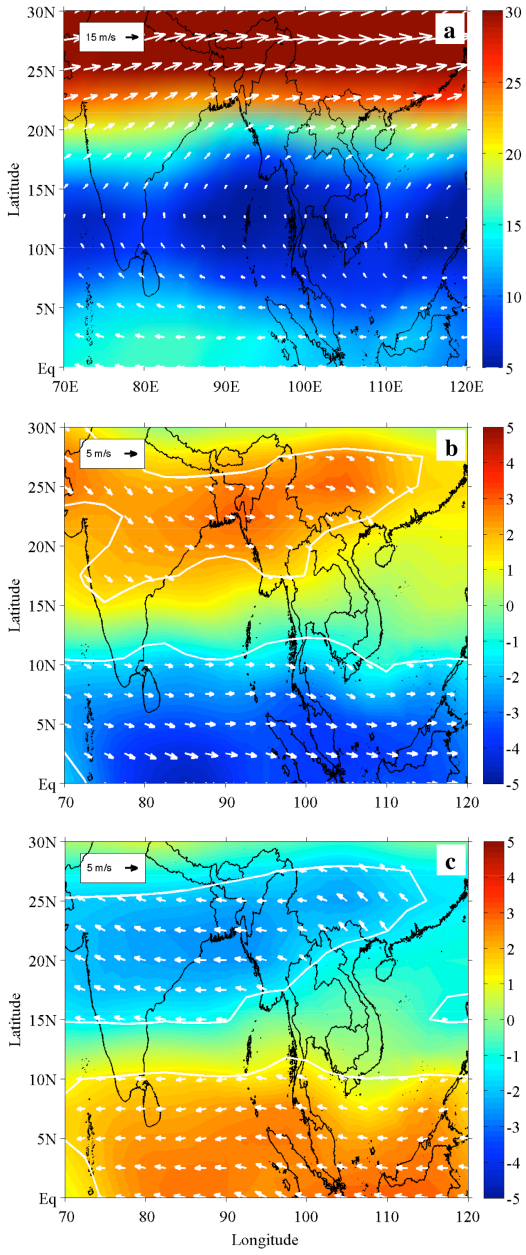

Figure 2.7: Post-monsoon season 200–850 hPa vertical wind shear (m s^{-1}) anomalies for (a) the 33-year mean, (b) anomalies during El Niño, and (c) anomalies during La Niña events. Regions enclosed by contouring represent differences in the anomalies between each ENSO phase and the 33-year mean at $p < 0.1$ using a Student's t test.

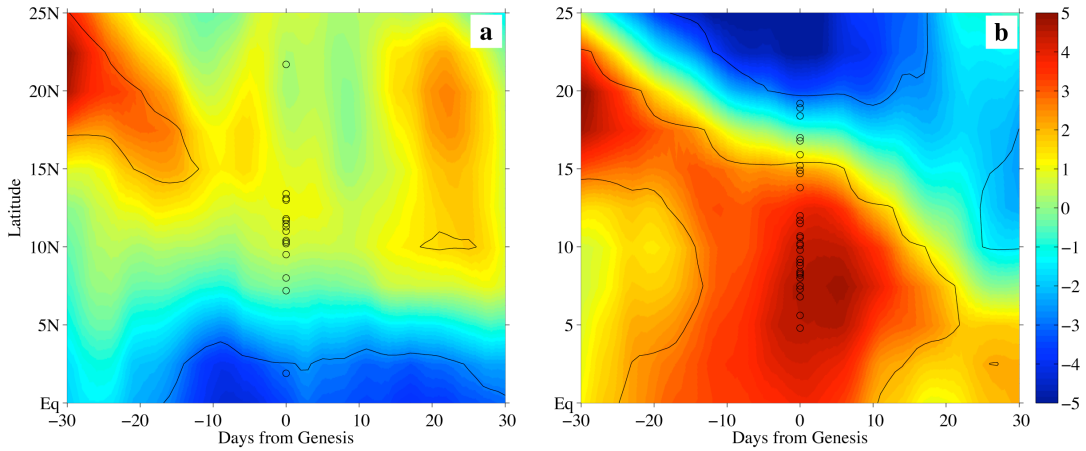

Figure 2.8: Time-latitude composite diagrams of deep layer wind shear (200-850 hPa) anomalies (m s^{-1}) during (a) El Niño and (b) La Niña events spanning a 60 day period relative to TC formation (± 30 days). The anomalies are based of the 33-year mean centered on the mean genesis date (day 314). The values for each point represent wind shear magnitude averaged every 2.5° of latitude between 80°E and 100°E. The genesis latitude of each storm is marked with an open circle. Day zero is reference to when the tropical cyclone first reached wind speeds of 20 kt (weak depression). Regions enclosed by contouring represent differences in the anomalies between (a) El Niño and (b) La Niña and the 33-year mean at $p < 0.1$ using a Student's t test.

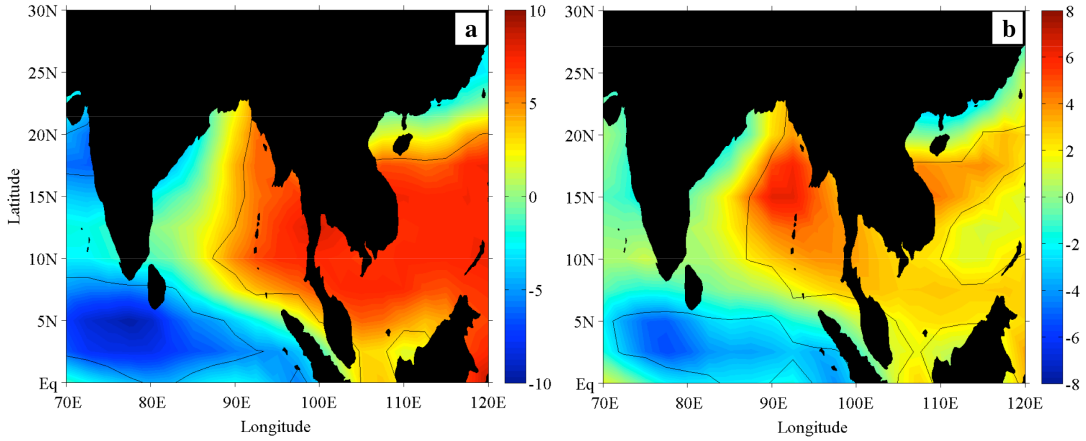

Figure 2.9: Difference (La Niña minus El Niño) between (a) 700 hPa and (b) 850 hPa post-monsoon season averaged relative humidity (%). Positive (negative) values represent higher values in the La Niña (El Niño) composites. Regions enclosed by contouring represent differences in the anomalies between each ENSO phase at $p < 0.1$ using a Student's *t* test.

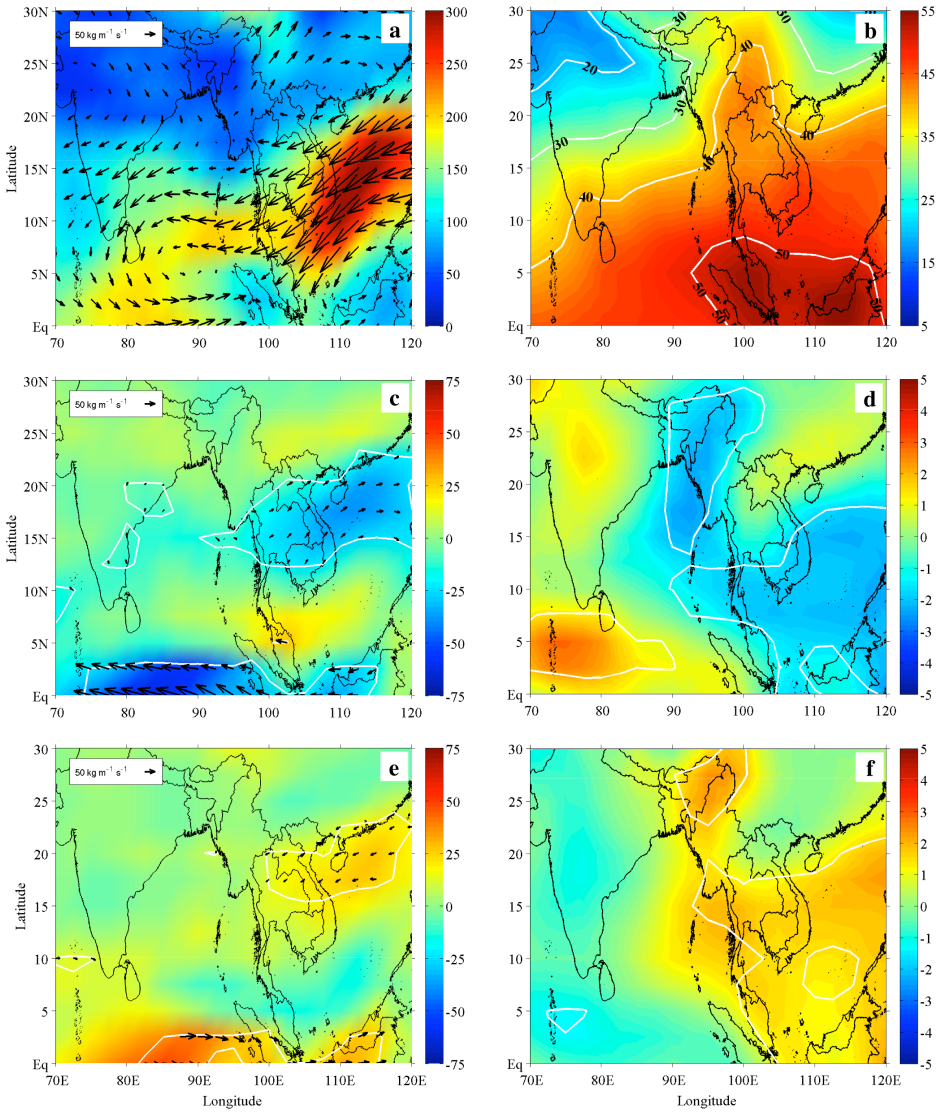

Figure 2.10: (Left: a,c,e) Vertically integrated moisture transport, **Q**, and vectors for (a) the 33-year mean, (c) anomalies during El Niño, and (e) anomalies during La Niña (kg m^{-1} s^{-1}). (Right: b,d,f) Same as left, except for precipitable water, W (kg m^{-2}). Regions enclosed by contouring represent El Niño (c,d) and La Niña (e,f) anomalies that vary significantly from the 33-year mean (p value <0.1, Student's t test).

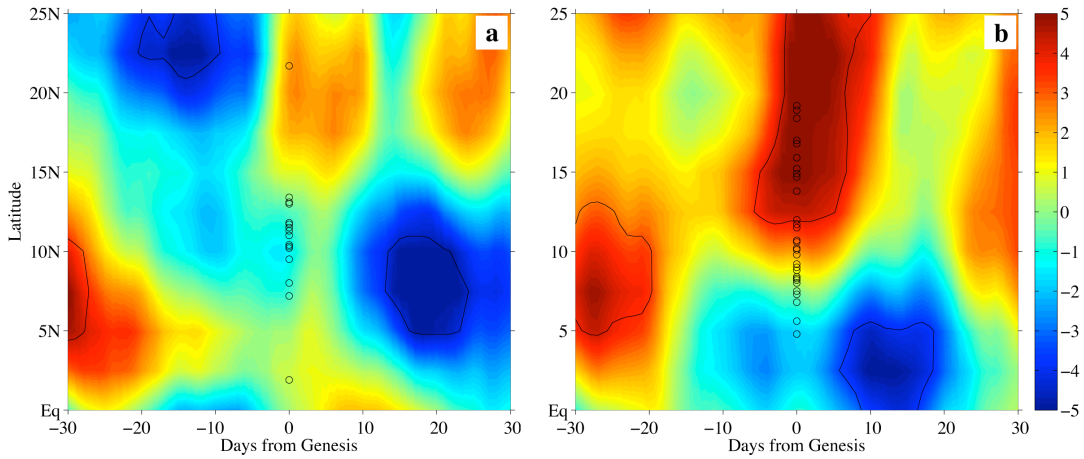

Figure 2.11: Time-latitude composite diagrams of 600 hPa relative humidity anomalies (%) during (a) El Niño and (b) La Niña events spanning a 60 day period relative to TC formation (± 30 days). The anomalies are based of the 33-year mean centered on the mean genesis date (day 314). The values for each point represent the humidity averaged every 2.5° of latitude between 80°E and 100°E. The genesis latitude of each storm is marked with an open circle. Day zero is reference to when the tropical cyclone reached wind speeds of 20 kts (weak depression). Regions enclosed by contouring represent differences in the anomalies between (a) El Niño and (b) La Niña and the 33-year mean at $p < 0.1$ using a Student's t test.

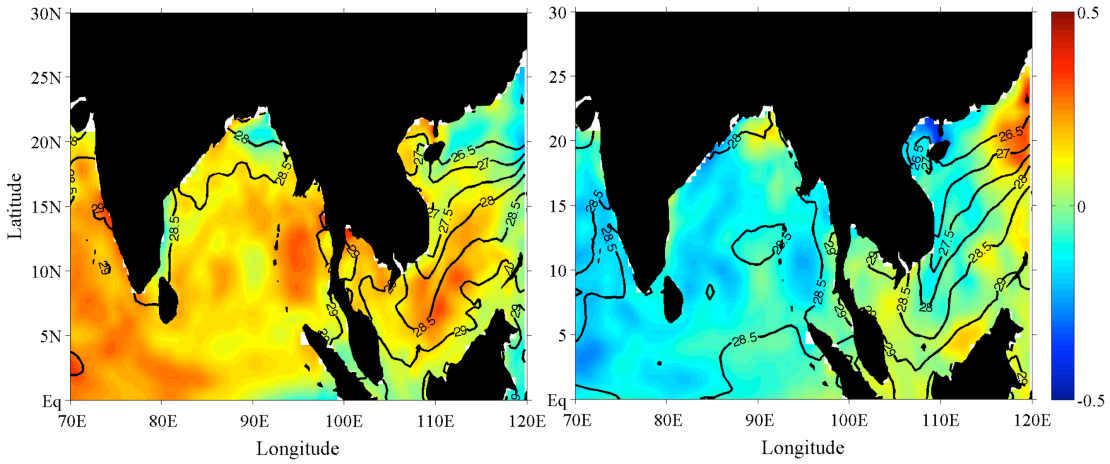

Figure 2.12: SODA SSTA (°C) composites for (a) El Niño and (b) La Niña events. Warm (cool) regions indicate higher (lower) SSTAs during each respective ENSO phase. SSTs during El Niño and La Niña are contoured at a 0.5°C interval.

CHAPTER 3

ESTIMATIONS OF THE BARRIER LAYER THICKNESS IN THE INDIAN OCEAN USING AQUARIUS SALINITY AND HYCOM SIMULATIONS[2]

[2]Felton, C. S., B. Subrahmanyam, V. S. N. Murty, and J. F. Shriver, (submitted December 2013): Estimation of the Barrier Layer Thickness in the Indian Ocean using Aquarius Salinity and HYCOM. *J. Geophys. Res.,* (submitted).

ABSTRACT

Monthly barrier layer thickness (BLT) estimates are derived from satellite measurements using a multilinear regression model (MRM) and HYbrid Coordinate Ocean Model (HYCOM) simulations for the Indian Ocean. The recently launched Soil Moisture and Ocean Salinity (SMOS) and Aquarius SAC-D salinity missions are currently supplying global measurements of sea surface salinity (SSS) at time scales that were previously unobtainable. The MRM relates BLT to sea surface salinity (SSS), sea surface temperature (SST) and sea surface height anomalies (SSHA) is developed. Three regions are selected to evaluate the performance of the MRM where the BLT variability is most rigorous, the Southeast Arabian Sea (SEAS), Bay of Bengal (BoB), and Eastern Equatorial Indian Ocean (EEIO) during 2012-2013. It is shown that different mechanisms are important for sustaining the BLT variability in each of the selected regions. Results suggest that salinity measurements obtained from Aquarius and SMOS can be useful for tracking and predicting the BLT in the Indian Ocean. Larger MRM errors occur along coastlines and near islands where land contamination skews the satellite SSS retrievals. The evolution of the BLT from 2012 to 2013, as well as the advantages and disadvantages of the current model are discussed. BLT estimations using HYCOM simulations display large errors that could be related to the model layer structure and BLT methodology. The MRM model is also shown to be useful for investigating the BLT variability in the Indian Ocean due to the Indian Ocean Dipole (IOD) events.

3.1. INTRODUCTION

Salinity stratification and subsequent barrier layer (BL) formation play an important role in regulating surface heat exchanges. Sharp salinity gradients increase the stability of the water column and inhibit mixing of cool thermocline waters into the warm surface waters. This limits heat exchange and allows for upper ocean temperatures to warm (Monetégut et al. 2007; Sengupta et al. 2008; Girishkumar et al. 2013). When the ocean is stratified by salinity, there is a difference between isothermal layer depth (ILD) and mixed layer depth (MLD). The ILD is typically determined by a temperature criterion while the MLD is obtained using the density criterion. The barrier layer thickness (BLT) is defined as the difference between the ILD and MLD.

Sprintall and Tomczak (1992) were the first to study the BL on a global scale and determined that the formation of the BL in the Indian Ocean is driven by the monsoon cycle. Reversing winds, currents, and freshwater fluxes (Evaporation (E), precipitation (P), and river runoff (R)) each play a role in the formation of the BL across the basin (Masson et al. 2002; Qu et al. 2005; Durand et al. 2007; Thadathil et al. 2007; Thadathil et al. 2008). Equatorial waves also impact the formation of the BL due to the alterations in the thermocline depth (Girishkumar et al. 2011).

The launch of National Aeronautics and Space Administration's (NASA) Aquarius Salinity/SAC-D and European Space Agencies (ESA) Soil Moisture Ocean Salinity (SMOS) missions has allowed for global SSS measurements to be made on spatial and temporal scales that were previously logistically impossible. Both satellites have already been able to reveal the SSS structure of many phenomena including tropical instability waves (Lee et al. 2012), a haline hurricane wake from the Amazon River plume (Grodsky

et al. 2012), surface freshening events in the Pacific (Boutin et al. 2013), the seasonality of salt flux in the Indian Ocean (Nyadjro et al. 2013; Subrahmanyam et al. in review), and the Madden-Julian Oscillation (Grunsiech et al. 2013) and the Indian Ocean Dipole (Nyadjro and Subrahmanyam, 2014).

While Argo buoys have drastically increased the number of temperature and salinity measurements in ocean basins, relatively poor spatial (single point measurement) and temporal (~10 day resurface time) coverage makes tracking the barrier layer in near-real time a difficult task. With satellites now providing global coverage of SSS on short time scales (3 days - weekly), we investigate the feasibility of using satellite-derived variables to estimate the BLT in the Indian Ocean. While this paper focuses on monthly computations, it sets the stage for future work as the accuracy of the salinity measuring satellites improves at higher temporal resolution. Comparisons between BLT determined from gridded Argo float profiles and estimates using a multilinear regression model for three regions in the Indian Ocean are performed. The advantages and disadvantages of the technique are described as well. Simulations from the HYbrid Coordinate Ocean Model (HYCOM) are also used to evaluate the performance of the MRM. The organization of the paper is as follows. Data sources and methodology are presented in section 2 followed by the results in section 3. Section 4 summarizes the results and discusses the implications for using Aquarius and SMOS SSS measurements to understand and track the BL in the Indian Ocean.

3.2. DATA AND METHODOLOGY

a. Data Sources

Monthly Aquarius SSS version 2.0 Level 3 data from September 2011 to August 2013 are obtained from NASA's Jet Propulsion Laboratory (JPL). In order to produce the Level 3 gridded maps, the converted Aquarius sensor measurements (raw signal to SSS) are binned onto a 1° degree global grid. Mapped SSS products are computed as averages across all 3 radiometers as well as individual instrument files (daily to weekly to monthly). Monthly Aquarius SSS measurements, as a whole, agree well with SMOS, Argo, and HYCOM SSS with differences rarely exceeding ±1 PSU in the Indian Ocean (Subrahmanyam et al. in review). Monthly composite, 1° resolution Level 3 SMOS SSS data were obtained from the Ocean Salinity Expertise Center (CECOS) of CNES (Centre National d'Etudes Spatiales)-Ifremer Centre Aval de Traitement des Données SMOS (CATDS), located in Plouzane, France. Both satellites' onboard passive microwave radiometers estimate salinity from sea surface brightness temperature using the L-band (1400-1427 MHz) frequency. Since some gaps are present in the monthly gridded values, an inverse weighted function is used to fill missing open ocean values within 1° degree (8 surrounding points).

Monthly gridded Argo temperature and salinity profiles from January 2005 to July 2013 are obtained from the Asia Pacific Data-Research Center (APDRC). The data center produces monthly gridded 1° resolution files from individual float measurements by using a variational interpolation algorithm to minimize the misfit between the interpolated fields and the individual float profiles. MLD and ILD are determined from the gridded data using the criteria by Sprintall and Tomczak (1992). The ILD is defined

at the depth where the temperature at depth (T_z) reaches ±0.5°C from the surface value (T_0); in this way the presence of thermal inversions (up to +0.5°C) are considered. MLD is defined using a variable density criterion as follows:

$$\Delta\sigma = \sigma_t(T_0 + \Delta T, S_0, P_0) - \sigma_t(T_0, S_0, P_0) \quad (1)$$

where $\Delta\sigma$ is the difference in density from the surface to the base of the MLD. The first term on the right is the density equal to a change in ΔT (+0.5°C) from the surface temperature while keeping salinity constant, and the second term on the right is the surface σ_t value (kg m^{-3}). The MLD is then found by searching each profile to find where σ_t is equal to surface $\sigma_t + \Delta\sigma$. If the density value falls between two Argo levels, linear interpolation is used to estimate the exact depth (m). The BLT is then defined as the difference between the ILD and MLD (ILD - MLD = BLT).

HYCOM simulations for year 2012 were obtained from the real-time data assimilative 1/12º global HYCOM nowcast/forecast system. It is a next-generation system capable of nowcasting and forecasting the oceanic "weather." Some components include the three-dimensional ocean temperature, salinity and current structure, the surface mixed layer, and the location of mesoscale features such as eddies, meandering currents, and fronts. The system used 3-hourly forcing from the Navy Operational Global Atmospheric Prediction System. The data assimilation was performed using the Navy Coupled Ocean Data Assimilation (NCODA) (Cummings 2005) system with a model forecast as the first guess. NCODA assimilates available satellite altimeter observations (along track obtained via the NAVOCEANO Altimeter Data Fusion Center), satellite and in-situ sea surface temperature (SST) as well as available in-situ vertical temperature and salinity profiles from XBTs, ARGO floats and moored buoys. For additional details on

the HYCOM nowcast/forecast system the reader is referred to Metzger et al. (2009). MLD, ILD, and BLT were determined from HYCOM simulations using the same methodology as used for Argo.

Monthly Archiving, Validation, and Interpretation of Satellite Oceanographic (AVISO) sea surface height anomalies (SSHA) data from January 2005 to July 2013 at 1/3° degree resolution are used as a proxy for thermocline depth in the regression formula. National Oceanic and Atmospheric Administration (NOAA) optimally interpolated monthly sea surface temperature (NOAA OI SST v2) data from January 2005 to July 2013 are also used. The SST monthly fields are derived by a linear interpolation of the weekly optimum interpolation (OI) version 2 fields to daily fields then averaging the daily values over a month with a 1° horizontal resolution (Reynolds et al. 2002).

b. Methodology

Since satellite measurements are restricted to measuring the surface micro-layer (top mm), a multilinear regression model is used to relate the remotely sensed products to the BLT. First, all products are linearly interpolated onto a 1° x 1° degree common grid. The multilinear regression model (MRM) for estimating the BLT is as follows:

$$BLT = b_0 + \alpha_1 SSS + \alpha_2 SST + \alpha_3 SSHA \tag{2}$$

where b_0 is the constraint term and $\alpha_{1,2,3}$ are the coefficient weights. The constraint term (b_0) and each of the coefficients (α_i) are computed from the 2005-2011 Argo SSS, OISST, and AVISO SSHA values for each month at each grid point. SSS and SST are both related to upper ocean stratification and are included as proxies for the MLD. SSHAs from AVISO are used as a proxy for thermocline depth (or ILD) as studies have

illustrated the connection between the two (e.g. McPhaden and Nagura 2013). Reconstructions of BLT are then created using monthly Argo SSS and remotely sensed SSS products (Aquarius and SMOS) with OISST and AVISO SSHAs. A pictorial diagram of the methodology has been included (Figure 3.3).

3.3. RESULTS

a. Validation of Data Sources

Before utilizing the model, each salinity data source is briefly validated. The distribution of salinity in the Indian Ocean is unique when compared to the other basins with higher salinities in the Arabian Sea contrasted by lower salinity in the Bay of Bengal (Figure 3.1). Aquarius is able to capture both the spatial pattern and seasonal cycle well (Figure 3.2). In the Arabian Sea, evaporation (E) greatly exceeds precipitation (P) resulting in higher salinity (>36 PSU). Strong seasonal monsoon winds and the large air-sea moisture gradient result in high evaporation rates and higher salinity. Lower salinity (<34 PSU) is found in the eastern side of the basin. Freshwater inputs into the Bay of Bengal, via river runoff and precipitation, drive very low salinities (Sengupta et al. 2006). Salinity is also low along the Sumatra coastline due to enhanced rainfall and input of low salinity waters from the Indonesian Throughflow (ITF). Seasonal reversing monsoonal winds also cause waters between the AS and BoB to exchange (Rao and Sivakumar 2003; Thadathil et al. 2007; Vinayachandran et al. 2013). During the southwest monsoon season (June-September), the strong eastward flowing South Monsoon Current transports saltier water from the AS into the BoB (Figure 3.2b) (Murty et al. 1992). A signature of this can be seen north of the equator from 60°E to 95°E in Figure 1 (~35 PSU). During the winter monsoon season (January-April) the flow reverses, becoming westerly. The

equatorward flowing East India Costal Current (EICC) carries freshwater from the BoB towards the westward flowing North Equatorial Current (NEC) into the Arabian Sea (Figure 3.2a). Consistent differences exist between Argo and the other sources in the SEAS region (Table 3.1). In the EEIO, salinity holds nearly constant through the year (Figure 3.2c). A slight drop occurs in October and November as the ITCZ begins to shift southward, bringing enhanced rainfall over the region.

b. BLT seasonal cycle

Distinctly different processes drive the seasonal cycle of the BLT in each of the three study areas. In the SEAS region, the BLT is driven by the seasonal influx of low saline waters from the BoB (Durand et al. 2007). During the winter months (January-March) low saline waters are advected around Sri Lanka shoaling the MLD, while the downwelling of salty AS water by Rossby waves deepen the ILD resulting in a thick BL (Figure 3.4a). The termination of the BL begins with the onset of the summer monsoon when high salinity waters arrive via the equatorward flowing West India Coastal Current (WICC) and remotely forced upwelling Rossby wave fronts (Shenoi et al. 2004, 2005). The BL in the BoB also peaks during the winter months (December – March), due to the redistribution of low saline waters from river runoff and precipitation (Figure 3.4b). The thin BLT in the BoB during April-November supports the development of weather disturbances such as tropical cyclones and monsoon depressions. The freshwaters cause strong density stratification in the upper ocean that shoals the MLD while Ekman pumping causes the ILD to deepen (Thadathil et al. 2006). In the EEIO, the BL peaks from November to January (Figure 3.4c), during the boreal winter period. The combined action of vertical and zonal advection off Sumatra, creating a subsurface salinity

maximum, and zonal advection by the seasonal Wyrtki jet, introducing a low saline surface layer from the ITF, causes the BL to develop (Masson et al. 2002).

c. MRM & HYCOM Results

With the validity of the salinity data sources confirmed (see Table 3.1, Figure 3.2), the rest of the paper focuses on the results from the regression model. Correlations were run between each of the selected BLT proxy terms (SSS, SST, and SSHA) and the MLD, ILD, and BLT from Argo data. This is done to ensure that the selected parameters can effectively estimate the BLT in each of the study areas. In the SEAS region (Table 3.2), SSS (SST) has high positive (negative) correlations during the boreal southwest monsoon and winter monsoon months with the MLD. The positive correlations with SSS indicate that salinity is important for stratification in this region with higher (lower) salinity creating a deeper (shallower) MLD. The negative relationship between the MLD and SST reveals that higher temperatures result in a shallower MLD due to upper ocean stratification. For much of the year, the ILD and SSHA are positively correlated, implying that a deeper ILD is associated with higher SSHAs, which is physically accurate. MLD and SSHA relationships vary with the monsoon seasons. Just prior to and during the summer monsoon (April – September), the two are negatively related while during the winter monsoon (October – March). The BLT is positively correlated and significantly with ILD and negatively correlated with MLD. In other words, the relationship shows that the shallower (deeper) the MLD (ILD), the thicker the BL is. The poor correlations between SSS, SST, and SSHA with MLD and ILD during March – April is likely due to the transitions between the winter and summer monsoon seasons

when other factors, such as wind stress and reversing currents, may be driving upper ocean processes.

Similar relationships are found between the MLD and SSS in the BoB as well (Table 3.3). Strong positive relationships indicate that salinity plays an important role in controlling the MLD year round, while the MLD and SST correlations vary with the monsoon season. During the summer monsoon (May – October), strong winds mix the upper ocean that keep temperatures cool and the mixed layer deep. During the winter, warmer temperatures allow for the MLD to deepen. The correlations between SSHA and the ILD also show relatively higher positive values around the southwest monsoon season. As in the SEAS, the MLD (ILD) holds strong negative (positive) relationships with the BLT throughout much of the year.

Positive correlations are prevalent from boreal summer to winter to spring months (August-April, except in December) between the MLD and SSS in the EEIO (Table 3.4). Negative correlations are present between the MLD and SST for the same months. This indicates that increased (or deceased) salinity and decreased (or increased) temperatures lead to ML shoaling. The correlations between the ILD and SSHA also show relatively higher positive values for almost all the months (except June). The strong positive correlations are due to the prominence of equatorial waves in this region, which have been shown to relate to SSHA and ILD oscillations (Hong et al. 2008). As in the other two regions, the BLT is positively correlated with the ILD and negatively correlated with the MLD. Due to the negative relationship between the BLT and MLD, this indicates that the shoaling of the MLD, coupled with the deepening of the ILD, leads to thick barrier layer formation.

Yearly averaged spatial patterns agree well between the Argo BLT (MLD-ILD) values (Figure 3.5a), each of the MRM estimations (Figure 3.5b, c, d), and HYCOM simulations (Figure 3.5e). Each of the MRMs are able to resolve thick barrier layer formation throughout the Indian Ocean including along the Sumatra coastline, in the Bay of Bengal, and in the SEAS region. Both satellite sources (Aquarius and SMOS) appear to overestimate the BLT in the SEAS region. The Aquarius results also indicate a thick barrier layer in the vicinity of the Sunda Strait (between Sumatra and Java) that is missing in the rest of the sources due to presence of a low salinity surface plume.

In order to investigate any seasonal trends, model estimates for each of the three-boxed regions were averaged for each month. During the boreal winter months, the BLT peaks in the SEAS region due to the influx of low saline water from the BoB (Figure 3.6a) and arrival of the second downwelling coastally trapped Kelvin wave (Nienhaus et al. 2012). Both Aquarius and SMOS overestimate the barrier layer thickness in February, September, and December (Figure 3.7a). The error peak during September may be due to enhanced rainfall over the region during the retreat of the SW monsoon that creates low salinities at the ocean surface, skewing the satellite SSS measurements. The presence of many small islands in the region (such as the Maldives) may also be skewing satellite SSS retrievals. Moving to the BoB, model estimations are comparatively much better (Figure 3.6b). Each model captures the seasonal cycle very well. The small differences between the profile derived Argo BLT and BLT using Argo SSS in the MRM are likely due to the linearity assumption (Figure 3.7b). It is also possible that the inclusion of an Ekman pumping term may improve the model estimations, but due to the lack of a continuous satellite record from a single sensor (2005-2013), this term was left out.

Future efforts could include wind stress from numerical weather prediction in order to account for this physical process. Errors in the EEIO are small as well (Figure 3.6c). The maximum error occurs in November when non-linear effects from equatorial waves may be causing the divergence between MRM estimations with Argo values (Figure 3.7c).

In order to show how the MRM can be used to estimate the BLT in near real-time the results have been extended into the first half of 2013 using the coefficients (b, α_i) defined earlier. Again spatial patterns are similar although the magnitudes vary (Figure 3.8). Again, errors in the SEAS region are highest in February (Figure 3.9a and 3.10a). Maximum errors are in the BoB during January (Figure 3.9b and 3.10b). EEIO errors are highest in March (Figure 3.9c and 3.10c).

d. Process Study

Understanding the BLT on monthly time frames also has implications for Indian Ocean Dipole (IOD) (Qiu et al. 2012; Guo et al. 2013), mixed layer heat budget (Girishkumar et al. 2013) and monsoon forecasting (Masson et al. 2005), as such the ability of the model to detect an IOD event is performed. During each IOD phase the BLT is altered by equatorial waves. A comparison between Argo (ILD-MLD), the Aquarius MRM, and HYCOM yields interesting results (Figure 3.11). The arrival of a downwelling Kelvin wave can be seen in the Argo and Aquarius BLT during September into October when the BLT increases rapidly. This occurs mainly due to a deepening of the ILD as the Kelvin wave arrives. The signal is also present in HYCOM but the magnitude and locations do not match well. The Aquarius regression model is also able to capture the BLT signal in November as it circumnavigates the BoB. While the understanding of the mechanisms for how the BLT impacts oceanic processes is still in

its infancy, as more detailed studies on the BLT are to be performed this study shows that Aquarius SSS can be used to estimate the BLT in the future. Tracking of the BLT should also improve as remotely sensed SSS measurements are improved near coastal regions,

3.4. DISCUSSION AND CONCLUSIONS

Estimates of the barrier layer thickness in the Indian Ocean are shown utilizing satellite measurements for the first time. A multilinear regression model (MRM) is used to relate SSS, SST, and SSHA to the BLT. Due to the relatively poor temporal and spatial coverage of Argo buoys, as compared to satellite measurements, this method offers an alternative for computing the BLT in the Indian Ocean. The results from the model show that satellite salinity measurements can be used in such predictions. The model performs well in each of the three study regions, able to capture the seasonal cycle, but diverges from Argo derived BLT in the Southeast Arabian Sea. This is likely due to the complexity of surface and subsurface processes that are not linearly related to the BLT in this region. The regression model was also able to capture the BLT signature associated with the IOD and will be used in future studies. HYCOM is also shown to have difficulties representing the BLT in the Indian Ocean as a whole. This may be due to the development of thick isopycnal layers beneath the thinner surface z layers in areas of strong density stratification. The thicker layer alters the signature of this density stratification in model temperature and salinity profiles, which then impacts MLD and ILD. The addition of more near-surface model layers or the use of a different MLD/ILD criterion could overcome this issue, however for this study the definitions are kept constant across datasets (Argo and HYCOM) to ensure an accurate comparison.

Assimilating the satellite derived SSS into ocean models with mixing parameterizations schemes (HYCOM for example) could aid in determining and detecting the presence of a BL. This is important since the BLT plays an important role in the evolution and strength of the Indian Ocean Dipole (Qiu et al. 2012), the Indian summer monsoon (Masson et al. 2005), and tropical cyclones (Yu and McPhaden 2011; Balaguru et al. 2012). Given the success in this preliminary effort, future efforts will be directed towards assimilating satellite SSS into ocean circulation models to better resolve the BLT in the Indian Ocean. The continued improvement of satellite retrieved SSS accuracy will also aid in tracking river discharge in this dynamic region.

Table 3.1: Sea Surface Salinity (SSS) averaged in each selected region from September 2011 – July 2013 (PSU).

	AS	BoB	EEIO
Aquarius	35.22	32.70	33.98
SMOS	35.28	32.67	34.09
Argo	35.64	33.06	34.17
HYCOM	35.30	33.05	34.27

Table 3.2: Correlation coefficients of BLT with MLD and ILD and correlation of MLD and ILD with Argo Sea Surface Salinity (SSS), OI Sea Surface Temperature (SST), and AVISO Sea Surface Height Anomalies (SSHA) for the Southeast Arabian Sea (SEAS) study region. Bolded values indication correlations where the *p*-value < 0.01.

SEAS	MLD vs SSS	MLD vs SST	ILD vs SSHA	MLD vs BLT	ILD vs BLT	MLD vs SSHA
Jan	**0.70**	**-0.29**	**0.45**	**-0.71**	**0.66**	**-0.41**
Feb	**0.38**	**-0.26**	**0.32**	**-0.77**	**0.83**	**-0.35**
Mar	**0.38**	0.00	0.03	**-0.24**	**0.70**	**-0.20**
Apr	-0.05	0.03	0.05	-0.02	**0.66**	**0.15**
May	**-0.22**	**-0.34**	**-0.15**	0.08	**0.70**	**-0.11**
Jun	**0.29**	0.07	**0.43**	**0.27**	**0.75**	**0.38**
Jul	**0.67**	**-0.13**	**0.55**	**-0.41**	-0.01	**0.54**
Aug	**0.75**	**-0.46**	**0.55**	**-0.58**	**-0.28**	**0.57**
Sep	**0.54**	**-0.20**	**0.49**	**-0.65**	**-0.18**	**0.45**
Oct	-0.02	**-0.20**	**-0.28**	**-0.50**	**0.14**	**-0.34**
Nov	**0.34**	**0.18**	**0.37**	**-0.68**	**0.35**	**-0.16**
Dec	**0.64**	**-0.15**	**0.61**	**-0.66**	**0.56**	**-0.15**

Table 3.3: Correlation coefficients of BLT with MLD and ILD and correlation of MLD and ILD with Sea Surface Salinity (SSS), Sea Surface Temperature (SST), and Sea Surface Height Anomalies (SSHA) for the Bay of Bengal (BoB) study region. Bolded values indication correlations where the *p*-value < 0.01.

BoB	MLD vs SSS	MLD vs SST	ILD vs SSHA	MLD vs BLT	ILD vs BLT	MLD vs SSHA
Jan	**0.63**	**0.37**	**0.13**	**-0.72**	**0.90**	**-0.10**
Feb	**0.66**	**0.48**	0.02	**-0.58**	**0.92**	**0.18**
Mar	**0.66**	**0.17**	0.01	**0.10**	**0.93**	**0.14**
Apr	**0.45**	**0.11**	0.07	**-0.17**	**0.62**	**0.20**
May	**0.60**	**-0.37**	**0.15**	0.08	**0.58**	**0.20**
Jun	**0.67**	**-0.27**	**0.20**	**-0.51**	**0.54**	0.04
Jul	**0.43**	**-0.09**	**0.25**	**-0.63**	**0.21**	**0.09**
Aug	**0.65**	**-0.11**	**0.19**	**-0.61**	0.06	-0.02
Sep	**0.72**	**-0.55**	**0.26**	**-0.62**	**0.18**	0.04
Oct	**0.51**	**-0.66**	**0.24**	**-0.48**	**0.61**	0.02
Nov	**0.57**	-0.01	**0.36**	**-0.65**	**0.86**	**-0.14**
Dec	**0.49**	**0.15**	**0.17**	**-0.59**	**0.84**	**-0.22**

Table 3.4: Correlation coefficients of BLT with MLD and ILD and correlation of MLD and ILD with Sea Surface Salinity (SSS), Sea Surface Temperature (SST), and Sea Surface Height Anomalies (SSHA) for the Eastern Equatorial Indian Ocean (EEIO) study region. Bolded values indication correlations where the *p*-value < 0.01.

EEIO	MLD vs SSS	MLD vs SST	ILD vs SSHA	MLD vs BLT	ILD vs BLT	MLD vs SSHA
Jan	**0.52**	**-0.28**	**0.36**	0.06	**0.93**	**-0.13**
Feb	**0.43**	**-0.49**	**0.44**	**0.08**	**0.75**	**0.46**
Mar	**0.31**	**-0.42**	**0.53**	**0.22**	**0.81**	**0.49**
Apr	**0.30**	**-0.13**	**0.56**	**-0.09**	**0.84**	**0.46**
May	**0.08**	**-0.14**	**0.54**	**-0.13**	**0.74**	**0.40**
Jun	**0.35**	**0.07**	**0.14**	**-0.29**	**0.55**	**0.33**
Jul	-0.05	**0.19**	**0.25**	**-0.36**	**0.45**	**0.09**
Aug	**0.26**	**0.12**	**0.35**	**-0.53**	**0.31**	**0.18**
Sep	**0.33**	-0.04	**0.51**	**-0.43**	**0.50**	**0.19**
Oct	**0.37**	**-0.26**	**0.67**	**-0.59**	**0.51**	**0.21**
Nov	**0.30**	**-0.13**	**0.66**	**-0.24**	**0.75**	**0.38**
Dec	0.05	0.02	**0.67**	**-0.11**	**0.87**	**0.43**

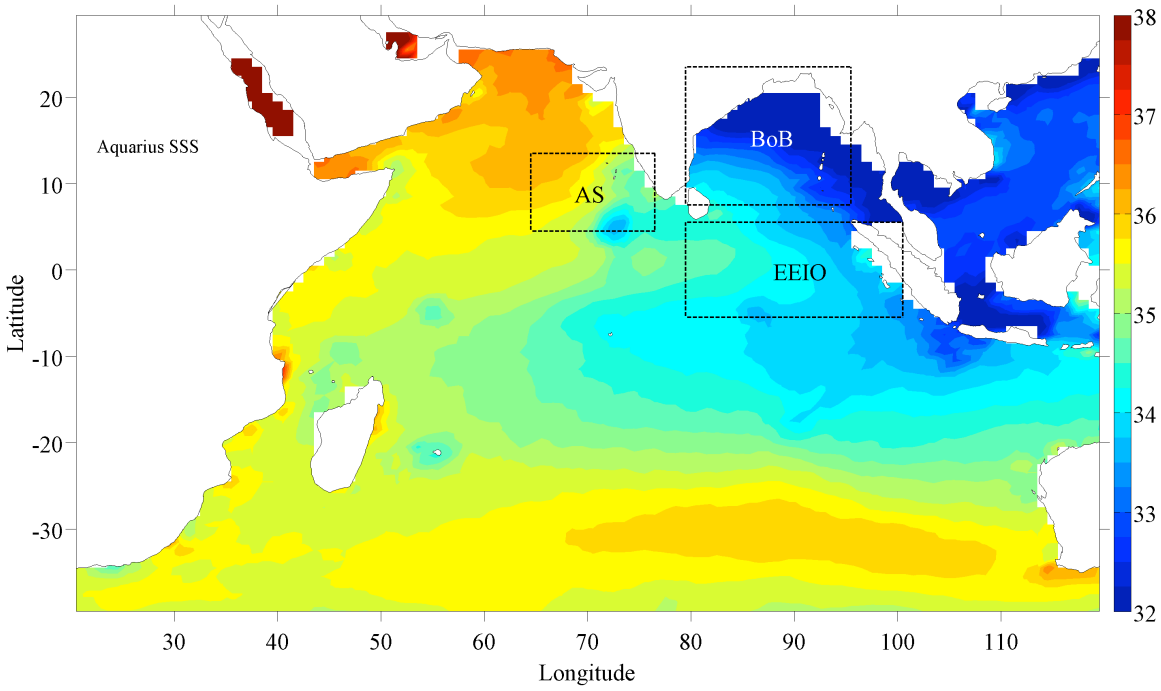

Figure 3.1: Level-3 Aquarius SSS (PSU) for the period from September 2011 - July 2013. Boxes indicate the regions where BLT estimates are compared. Shading interval is every 0.25 PSU.

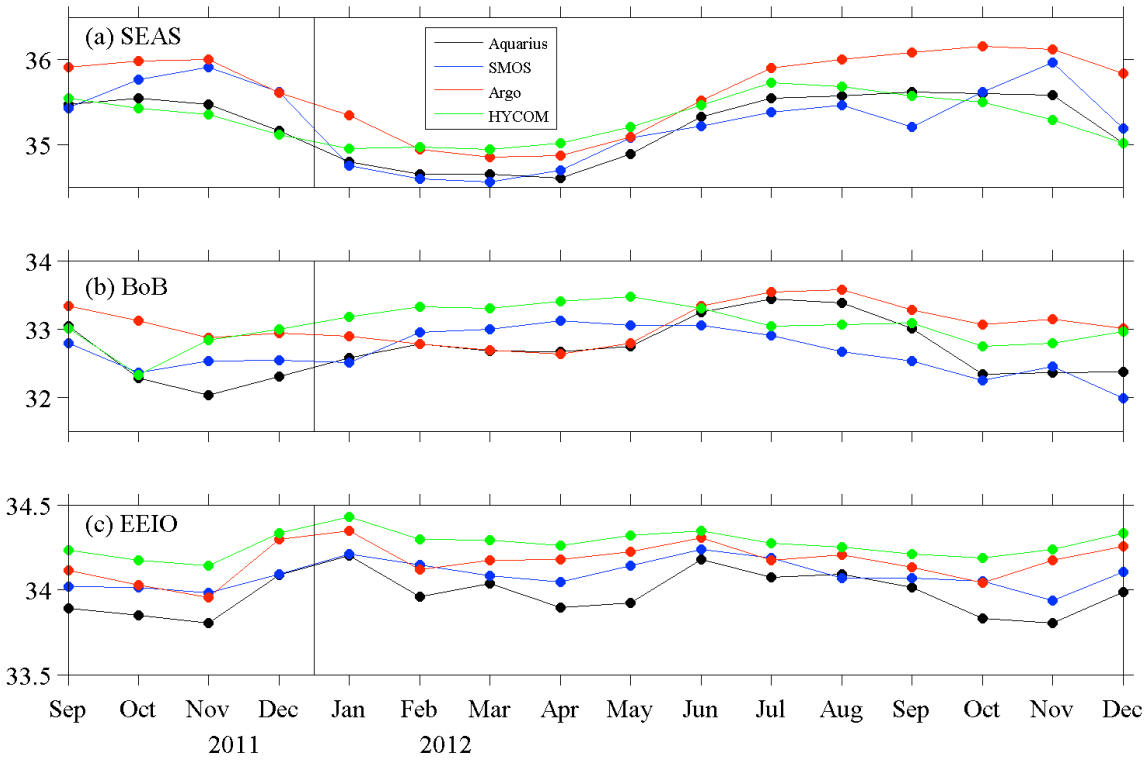

Figure 3.2: Comparison of the sea surface salinity (SSS) time-series during September 2011 – December 2012 in the (a) Southeast Arabian Sea, (b) Bay of Bengal, and (c) East Equatorial Indian Ocean boxed regions.

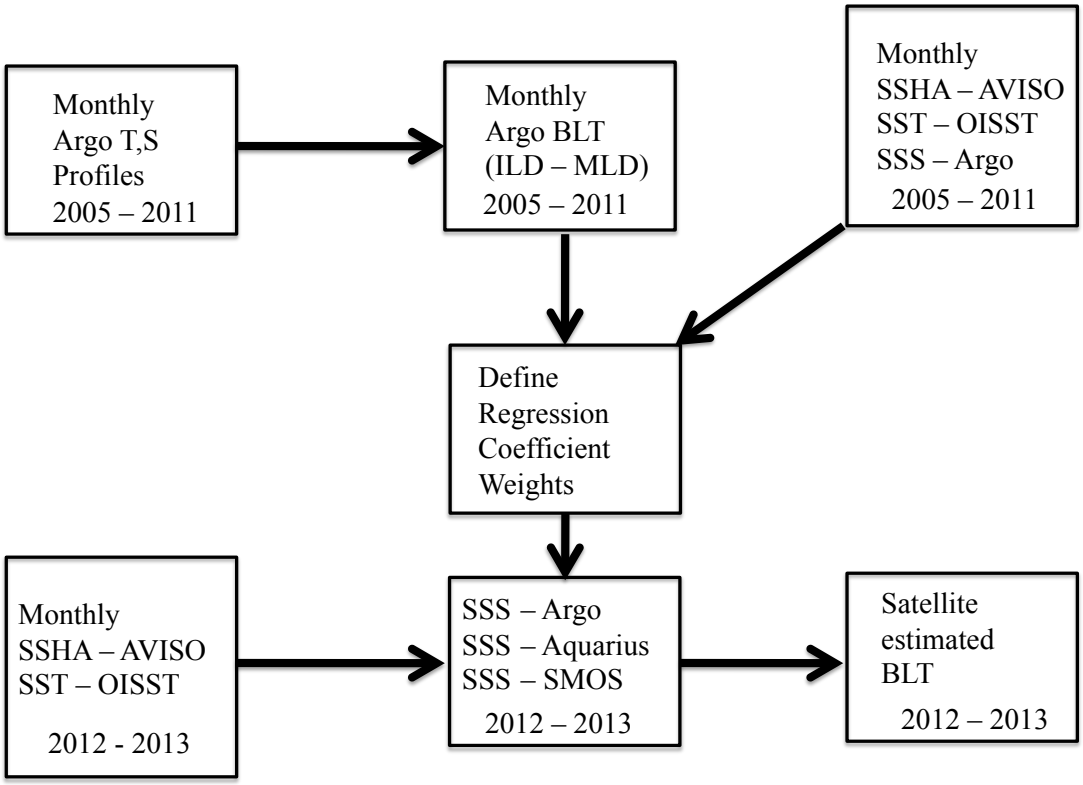

Figure 3.3: Methodology for creating BLT and regression estimated BLT.

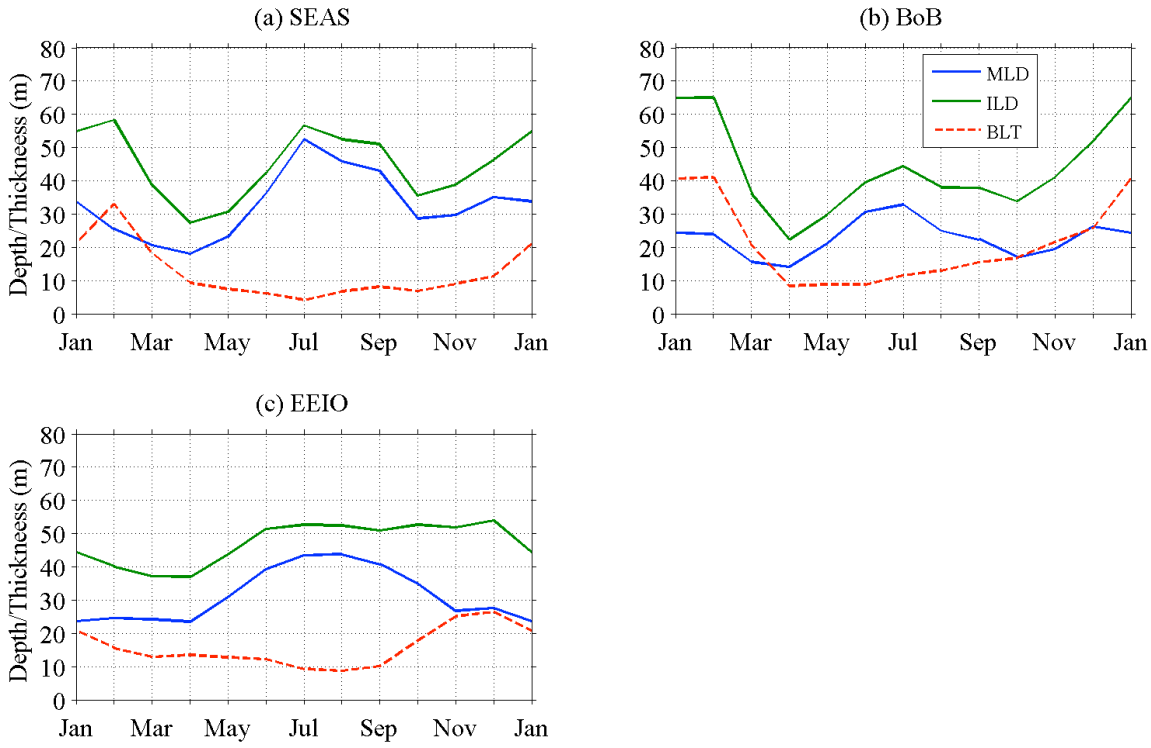

Figure 3.4: The seasonal evolution of the MLD (blue), ILD (green) and BLT (dashed red) for the (a) SEAS, (b) BoB, and (c) EEIO from Argo. January is shown twice to complete the seasonal cycle. BLT in the above figure is computed as the difference between the ILD and MLD (ILD-MLD).

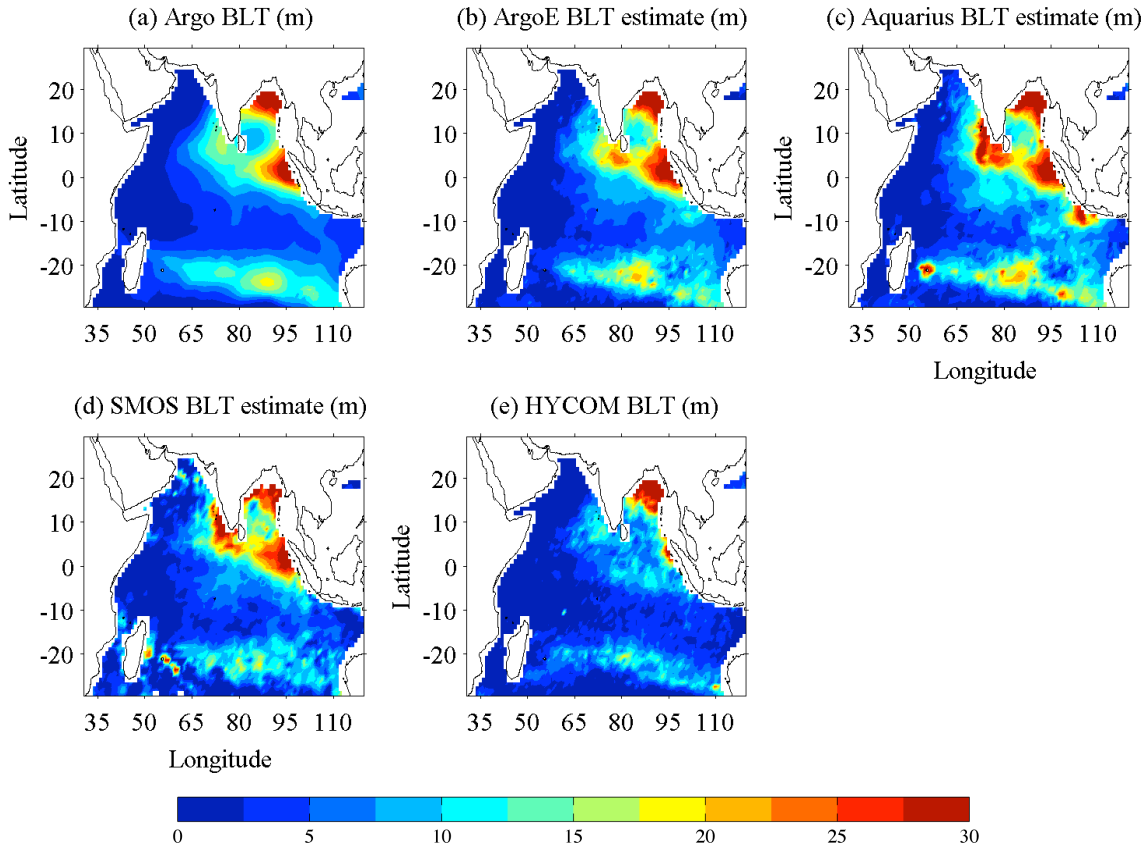

Figure 3.5: Annual mean BLT in the tropical Indian Ocean estimated from (a) Argo BLT (ILD-MLD, and (b) multilinear regression model BLT using Argo SSS (ArgoE), (c) using Aquarius SSS, (d) using SMOS SSS, and (e) using HYCOM. Shading interval is every 2.5 meters. SSHA and OISST are kept constant for b-d.

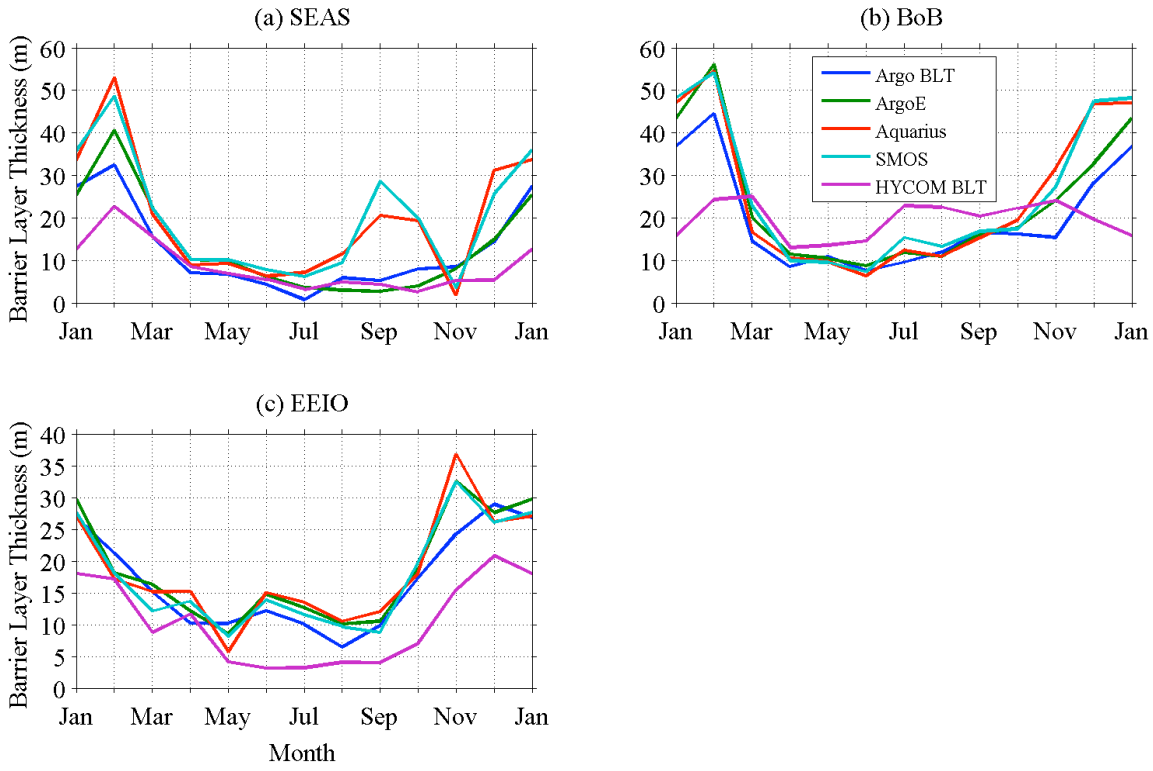

Figure 3.6: Seasonal cycles of box averaged BLT estimates in the year 2012 for (a) Southeast Arabian Sea, (b) Bay of Bengal, and (c) Eastern Equatorial Indian Ocean. January is shown twice to complete the seasonal cycle.

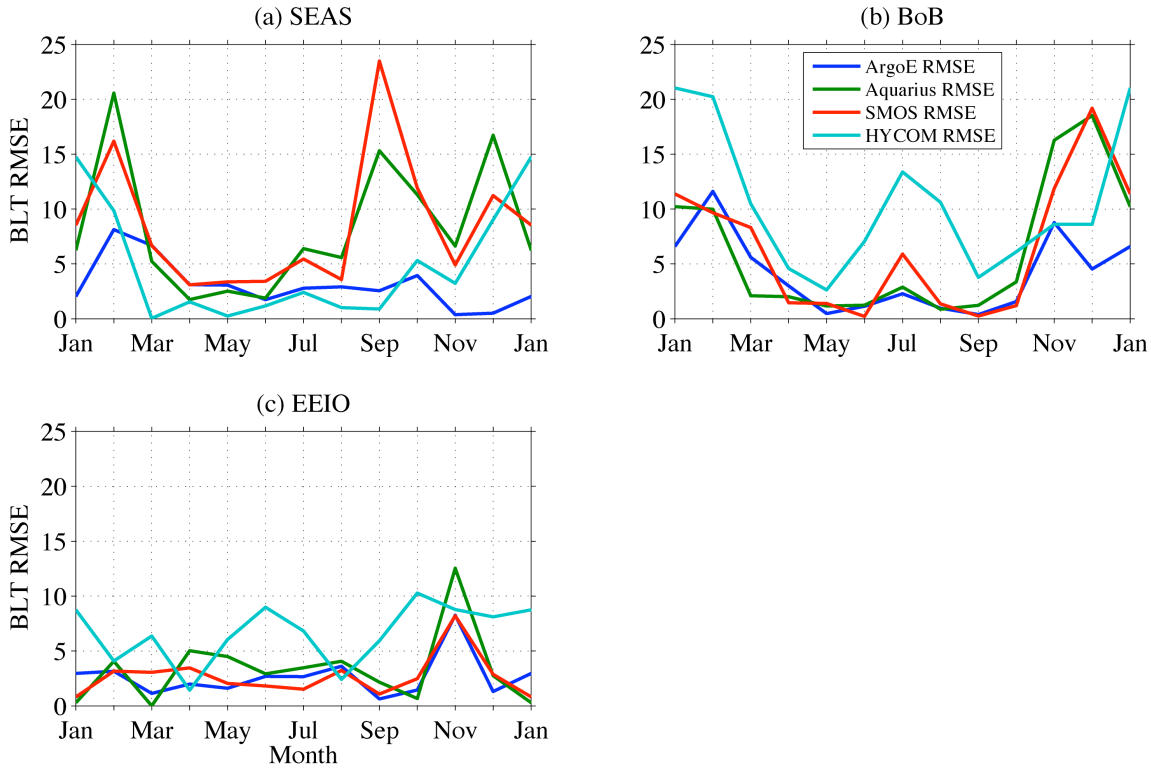

Figure 3.7: Seasonal cycles of box averaged BLT RMSE defined from the Argo BLT (ILD-MLD) for the year 2012 for the (a) SEAS, (b) BoB, and (c) EEIO. January is shown twice to complete the seasonal cycle. The Argo RMSE is between the estimated from the regression model and the Argo BLT (ILD-MLD).

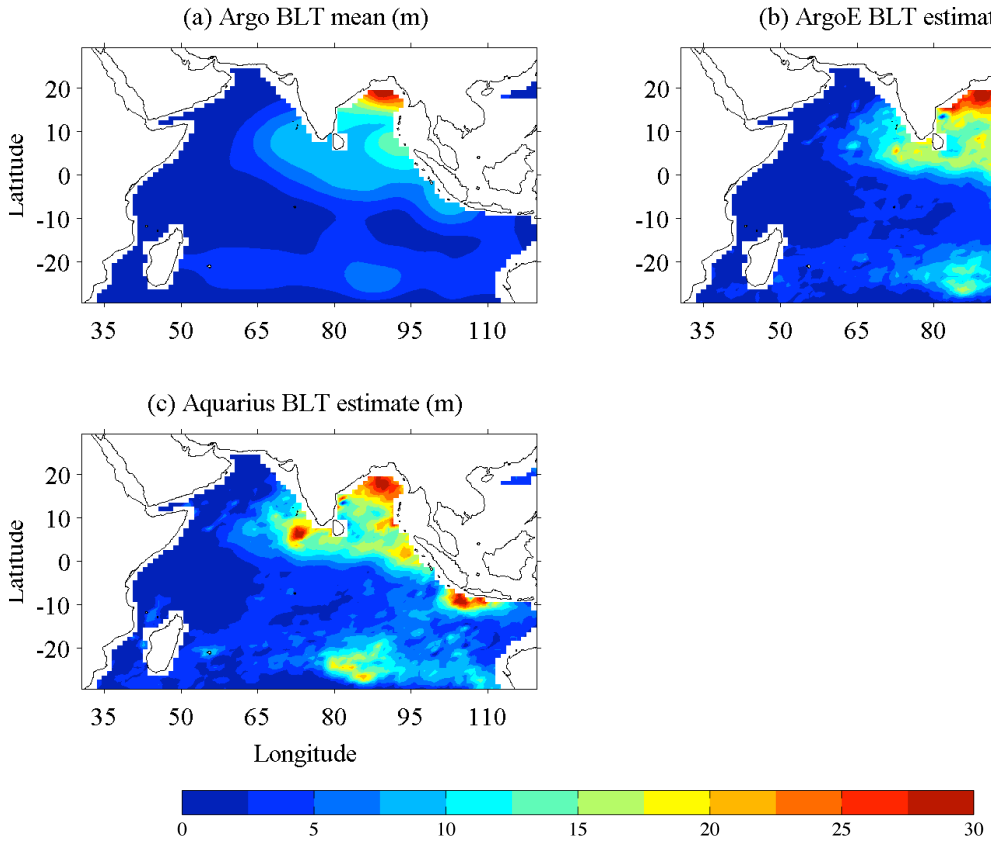

Figure 3.8: Barrier layer thickness (m) averaged from January – July of 2013. (a) Original Argo BLT from T, S profiles, (b) reconstructed for 2005-2011 coefficients for BLT using Argo SSS, and (c) Aquarius SSS. Shading interval is every 2.5 meters. BLT in (a) is the difference between ILD and MLD while in (b) it is estimated from the regression model.

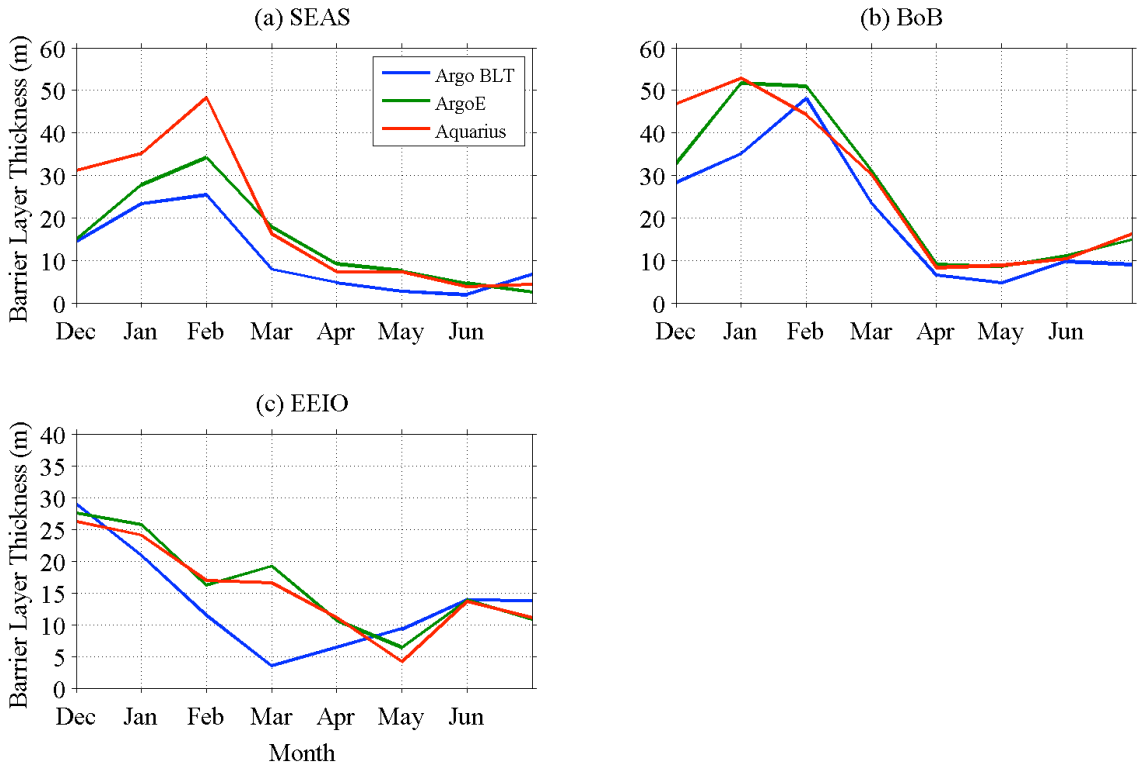

Figure 3.9: Boxed averaged BLT time-series (January – July 2013) for (a) SEAS, (b) BoB, and (c) EEIO.

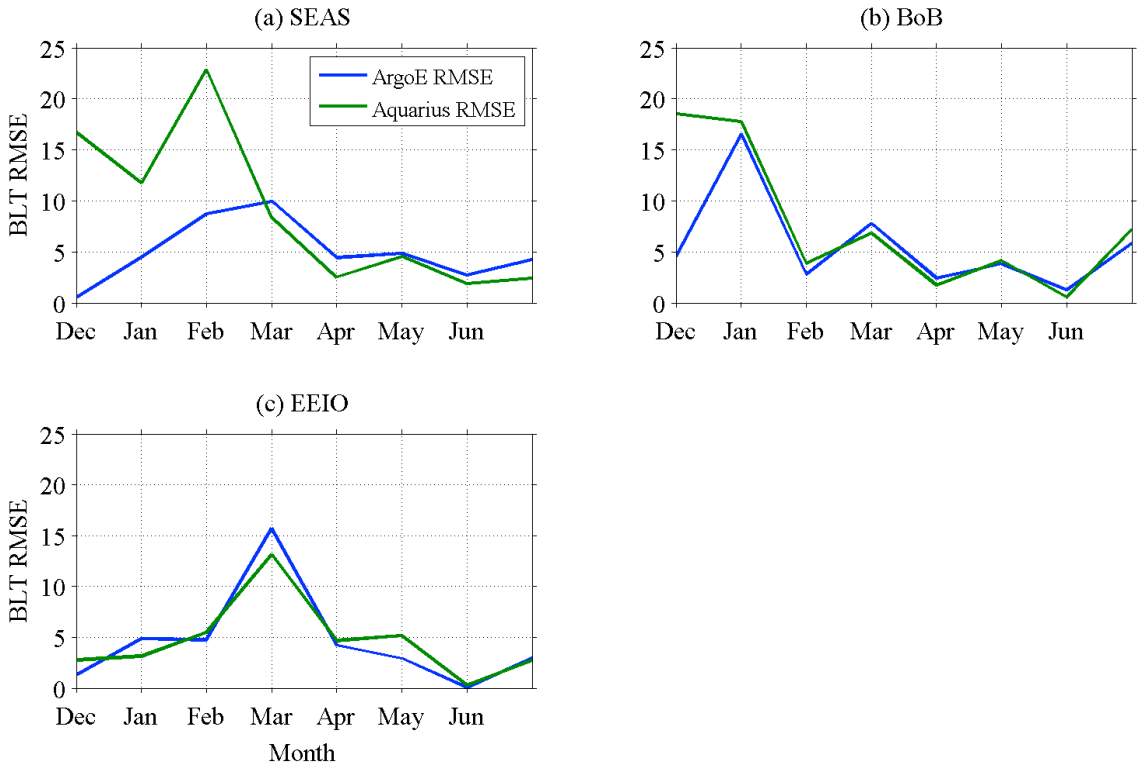

Figure 3.10: Boxed averaged BLT RMSE time-series (January – July 2013) for (a) SEAS, (b) BoB, and (c) EEIO.

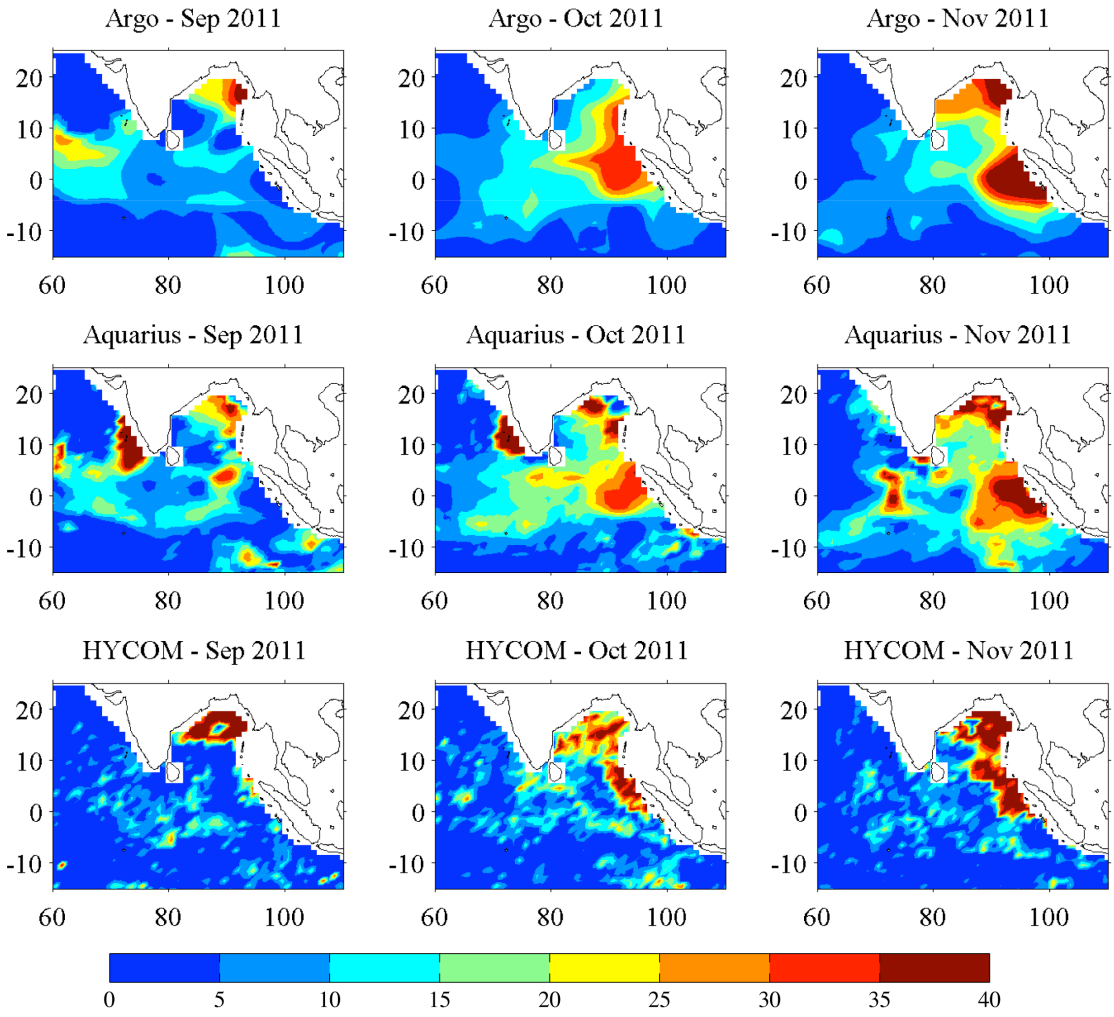

Figure 3.11: BLT evolution during the Positive IOD event in 2011 from (top) Argo BLT (ILD-MLD), the (middle) Aquarius Regression Model, and (bottom) HYCOM. Shading is every 5 m.

CHAPTER 4

CONCLUSIONS

This thesis is divided into two major research areas: 1. ENSO-modulated cyclogenesis over the Bay of Bengal and 2. Estimation of the Barrier Layer Thickness in the Indian Ocean using Aquarius Salinity and HYCOM simulations.

Oceanic and atmospheric conditions in the Indian Ocean are influenced by variabilities on multiple timescales. The modulations forced by these signals (ENSO, monsoons, IOD, ect.) cause alterations in tropical cyclone activity, the barrier layer thickness, salinity distributions, as well as other phenomena. It is important to investigate each of these features due their impacts on society and climate, both locally and globally.

The changes in the environment forced by ENSO are shown to explain the anomalous tropical cyclone activity during each phase. Large-scale patterns averaged over the post-monsoon season during La Niña events indicate enhanced cyclonic vorticity, higher shear over the equatorial and southern BoB, and greater relative humidity when compared to El Niño events (Felton et al. 2013). These conditions favor and partially explain the increase in tropical cyclone activity during La Niña events. The cooler SSTs during La Niña over the BoB indicate enhanced moisture transport into the lower atmosphere that further fuels tropical system development. Future research should investigate if ENSO altered Madden-Julian Oscillation patterns also influence tropical cyclone development due to the prevalence of the MJO during the post-monsoon season.

While the seasonal cycle of the barrier layer is known in the Indian Ocean, tracking the barrier layer in near-real time is difficult. A multilinear regression model (MRM) is developed that relates SSS, SST, and SSHA to the BLT. Due to the relatively poor temporal and spatial coverage of Argo buoys, as compared to satellite measurements, this method offers an alternative for computing the BLT in the Indian Ocean. MRM results show that satellite salinity measurements can be used in such predictions. The MRM performs well in each of the three study regions, able to capture the seasonal cycle, but diverges from Argo derived BLT in the Southeast Arabian Sea. This is likely due to the complexity of surface and subsurface processes that are not linearly related to the BLT in this region. The MRM is also able to capture the BLT signature associated with the IOD and should be used in future studies. HYCOM is also shown to have difficulties representing the BLT in the Indian Ocean as a whole. This may be due to the development of thick isopycnal layers beneath the thinner surface z layers in areas of strong density stratification. This thicker layer alters the signature of the density stratification in model temperature and salinity profiles, which then impacts the MLD and ILD. The addition of more near-surface model layers or the use of a different MLD/ILD criterion could overcome this issue, however for this study the definitions are kept constant across datasets (Argo and HYCOM) to ensure an accurate comparison.

Assimilating satellite derived SSS into ocean models with mixing parameterizations schemes (HYCOM for example) could aid in determining and detecting the presence of a BL. This is important since the BL plays an important role in the evolution and strength of many oceanic and atmospheric features in the Indian Ocean (Balaguru et al. 2012; Qui et al. 2012; Guo et al. 2013). Given the success in this preliminary effort, future efforts

should be directed towards assimilating satellite SSS into ocean circulation models to better resolve the BL in the Indian Ocean. The continued improvement of satellite retrieved SSS accuracy will also aid in tracking river discharge in this dynamic region. Real time comparisons with salinity from Argo floats and satellite retrievals may also shed light on upper ocean stratification processes, such as barrier layer erosion and surface (upper 5 meter) freshwater pool dynamics.

REFERENCES

Ashok, K., Z. Y. Guan, and T. Yamagata, 2001: Impact of the Indian Ocean dipole on the relationship between the Indian monsoon rainfall and ENSO. *Geophys. Res. Lett.*, **28**, 4499–4502.

Balaguru, K., P. Chang, R. Saravanan, L. R. Leung, Z. Xu, M. Li, and J.S. Hsieh, 2012: Ocean barrier layers' effect on tropical cyclone intensification. *Proc. Natl. Acad. Sci. U.S.A.*, **109** (36), 14343-14347, doi: 10.1073/pnas.1201364109.

Bhat, G. S., and collaborators, 2001: BOMEX: The Bay of Bengal monsoon experiment. *Bull. Amer. Meteorol. Soc.*, **82**, 2217–2243.

Bjerknes, J., 1969: Atmospheric Teleconnections from the Equatorial Pacific. *Mon. Wea. Rev.*, **97**, 63–172.

Bolton, D., 1980: The Computation of Equivalent Potential Temperature. *Mon. Wea. Rev.*, **108**, 1046–1053.

Boutin, J., N. Martin, G. Reverdin, X. Yin, and F. Gaillard, 2013: Sea surface freshening inferred from SMOS and ARGO salinity: impact of rain. *Ocean Sci.*, **9**, 183–192, doi: 10.5194/os-9-183-2013.

Camargo, S. J., K. A. Emanuel and A. H. Sobel, 2007: Use of a Genesis Potential Index to Diagnose ENSO Effects on Tropical Cyclone Genesis. *J. Climate*, **20**, 4819–4834.

Cummings, J.A., 2005: Operational multivariate ocean data assimilation. *Quart. J. Roy. Met. Soc.*, **131**, 3583-3604.

Durand, F., D. Shankar, C. de Boyer Montégut, S. S. C. Shenoi, B. Blanke, and G. Madec, 2007: Modeling the Barrier-Layer Formation in the Southeastern Arabian Sea. *J. Climate*, **20**, 2109–2120, doi: 10.1175/JCLI4112.1.

Emanuel, K. A. and D. S. Nolan, 2004: Tropical cyclone activity and global climate, Preprints, *26th Conf. on Hurricanes and Tropical Meteorology,* Miami, FL, Amer. Meteor. Soc., 240–241.

Felton, C. S., B. Subrahmanyam, V. S. N. Murty, 2013: ENSO-Modulated Cyclogenesis over the Bay of Bengal. *J. Climate*, **26**, 9806–9818. doi: http://dx.doi.org/10.1175/JCLI-D-13-00134.1

Giese, B. S., and S. Ray, 2011: El Niño variability in simple ocean data assimilation (SODA), 1871–2008. *J. Geophys. Res*., **116**, C02024, doi: 10.1029/2010JC006695.

Girishkumar, M. S., M. Ravichandran, M. J. McPhaden, and R. R. Rao, 2011: Intraseasonal variability in barrier layer thickness in the south central Bay of Bengal. *J. Geophys. Res.*, **116**, C03009, doi: 10.1029/2010JC006657

Girishkumar, M. S. and M. Ravichandran, 2012: The influences of ENSO on tropical cyclone activity in the Bay of Bengal during October-December. *Geophys. Res. Lett.*, **117**, C02033.

Girishkumar, M. S., M. Ravichandran, and M. J. McPhaden, 2013: Temperature inversions and their influence on the mixed layer heat budget during the winters of 2006–2007 and 2007–2008 in the Bay of Bengal. *J. Geophys. Res. Oceans*, **118**, doi: 10.1002/jgrc.20192.

Goswami, B. N., R. S. Ajayamohan, P. K. Xavier, and D. Sengupta, 2003: Clustering of synoptic activity by Indian summer monsoon intraseasonal oscillations. *Geophys. Res. Lett*., **30** (8), 1431.

Gray, W. M., 1968: Global View of the Origin of Tropical Disturbances and Storms. *Mon. Wea. Rev.*, **96**, 669–700.

Gray, W.M., 1998: The Formation of Tropical Cyclones. *Meteor. Atmos. Phys.*, **67,** 37-69.

Grodsky, S. A., N. Reul, G. Lagerloef, G. Reverdin, J. A. Carton, B. Chapron, Y. Quilfen, V. N. Kudryavtsev, and H.-Y. Kao, 2012: Haline hurricane wake in the Amazon/Orinoco plume: AQUARIUS/SACD and SMOS observations. *Geophys. Res. Lett.*, **39**, L20603, doi: 10.1029/ 2012GL053335.

Grunseich, G., B. Subrahmanyam, and B. Wang, 2013: The Madden-Julian oscillation detected in Aquarius salinity observations, *Geophys. Res. Lett.*, **40**, doi: 10.1002/2013GL058173.

Guo, F., Q. Lui, X-T. Zheng, and S. Sun, 2013: The Role of Barrier Layer in Southeastern Arabian Sea During the Development of Positive Indian Ocean Dipole Events. *J. Ocean Univ. China*, **12** (2), 245-252, doi: 10.1007/s11802-013-2170-4.

Hong, C-C., T. Li, LinHo, and J-S. Kug, 2008: Asymmetry of the Indian Ocean Dipole. Part I: Observational Analysis. *J. Climate*, **21**, 4834–4848. doi: 10.1175/2008JCLI2222.1.

Hong, C., T. Li, LinHo and Y. Chen, 2010: Asymmetry of the Indian Ocean Basinwide SST Anomalies: Roles of ENSO and IOD. *J. Climate*, **23**, 3563–3576.

Kanamitsu, M., W. Ebisuzaki, J. Woollen, S-K. Yang, J. J. Hnilo, M. Fiorino and G. L. Potter, 2002: NCEP–DOE AMIP-II Reanalysis (R-2). *Bull. Amer. Meteor. Soc.*, **83**, 1631–1643.

Kikuchi, K., B. Wang, and H. Fudeyasu, 2009: Genesis of tropical cyclone Nargis revealed by multiple satellite observations. *Geophys. Res. Lett.*, **36**, L06811.

Kikuchi, K. and B. Wang, 2010: Formation of Tropical Cyclones in the Northern Indian Ocean Associated with Two Types of Tropical Intraseasonal Oscillation Modes. *J. Meteor. Soc. Japan*, **88** (3), 475–496.

Kurihara, Y., M. A. Bender, R. E. Tuleya, R. J. Ross, 1990: Prediction Experiments of Hurricane Gloria (1985) Using a Multiply Nested Movable Mesh Model. *Mon. Wea. Rev.*, **118**, 2185–2198.

Lee, T., G. Lagerloef, M. M. Gierach, H.-Y. Kao, S. Yueh, and K. Dohan, 2012: Aquarius reveals salinity structure of tropical instability waves. *Geophys. Res. Lett.*, **39**, L12610, doi: 10.1029/2012GL052232.

Li, K., W. Yu, T. Li, V. S. N. Murty, S. Khokiattiwong, T. R. Adi, and S. Budi, 2013: Structures and mechanisms of the first-branch northward-propagating intraseasonal oscillation over the tropical Indian Ocean. *Climate Dyn.*, **40**, 1707-1720.

Li, Z., W. Yu, T.Li, V. S. N. Murty, F. Tangang, 2013: Bimodal Character of Cyclone Climatology in the Bay of Bengal Modulated by Monsoon Seasonal Cycle. *J. Climate*, **26**, 1033–1046.

Lin, I. I., C. H. Chen, I. F. Pun, W. T. Liu and C. C. Wu, 2009: Warm ocean anomaly, air sea fluxes, and the rapid intensification of tropical cyclone Nargis (2008). *Geophys. Res. Lett.*, **36**, L03817.

Maneesha, K., V. S. N. Murty, M. Ravichandran, T. Lee, W. Yu and M. J. McPhaden, 2012: Upper ocean variability in the Bay of Bengal during the tropical cyclones Nargis and Laila. *Prog. Oceanogr.,* **106**, 49-61.

Masson, S., P. Delecluse, J.-P. Boulanger, and C. Menkes, 2002: A model study of the seasonal variability and formation mechanisms of the barrier layer in the eastern equatorial Indian Ocean. *J. Geophys. Res.*, **107(C12)**, 8017, doi: 10.1029/2001JC000832.

Mason, S., at al., 2005: Impact of barrier layer on winter-spring variability of the southeastern Arabian Sea. *Geophys. Res. Lett.*, **32**, L07703, doi: 10.1029/2004GL021980.

McPhaden, M. J., G. R. Foltz, T. Lee, V. S. N. Murty, M. Ravichandran, G. A. Vecchi, J. Vialard, J. D. Wiggert and L. Yu, 2009: Ocean-Atmosphere Interactions During Cyclone Nargis. *EOS Trans. AGU*, **90(7)**, 53–60.

McPhaden, M, and M. Nagura, 2013: Indian Ocean dipole interpreted in terms of recharge oscillator theory. *Climate Dyn.*, 1432-0894, doi: 10.1007/s00382-013-1765-1.

Metzger, E.J., H.E. Hurlburt, A.J. Wallcraft, O.M. Smedstad, J.A. Cummings, E.P. Chassignet, 2009: “Predicting "Ocean Weather" Using the HYbrid Coordinate Ocean Model (HYCOM)”. Naval Research Laboratory, Washington DC Oceanography Division.

Montégut, C. B., J. Vialard, S. S. C. Shenoi, D. Shankar, F. Durand, C. Ethé, and G. Madec, 2007: Simulated Seasonal and Interannual Variability of the Mixed Layer Heat Budget in the Northern Indian Ocean. *J. Climate*, **20**, 3249–3268, doi: 10.1175/JCLI4148.1.

Murty, V. S. N., Y. V. B. Sarma, D. P. Rao, and C. S. Murthy, 1992: Water characteristics, mixing and circulation in the Bay of Bengal during southwest monsoon. *J. Mar. Res.*, **50**, 207 228.

Murty, V. S. N., Y. V. B. Sarma, and D. P. Rao, 1996: Variability of the oceanic boundary layer characteristics in the northern Bay of Bengal during MONTBLEX-90. *Earth Planet Sci*., **105**, 41–61.

Nienhaus, M. J., B. Subrahmanyam, and V. S. N. Murty, 2012: Altimetric Observations and Model Simulations of Coastal Kelvin Waves in the Bay of Bengal. *Marine Geodesy,* **35** (1), 190-216. doi: 10.1080/01490419.2012.718607

Nyadjro, E., B. Subrahmanyam, and B. S. Giese, 2013: Variability of salt flux in the Indian Ocean during 1960–2008. *Remote Sens. Environ.*, **134**, 175–193, doi: 10.1016/j.rse.2013.03.005.

Nyadjro, E. S., and B. Subrahmanyam, 2014: SMOS salinity mission reveals salinity structure of the Indian Ocean Dipole. *IEEE Trans. Geosci*., (in press).

Qiu, Y., W. Cai, L. Li, and X. Guo, 2012: Argo profiles variability of barrier layer in the tropical Indian Ocean and its relationship with the Indian Ocean Dipole. *Geophys. Res. Lett.*, **39**, L08605, doi: 10.1029/2012GL051441.

Qu, T., and G. Meyers, 2005: Seasonal variation of barrier layer in the southeastern tropical Indian Ocean. *J. Geophys. Res.,* **110**, C11003, doi: 10.1029/2004JC002816.

Rao, R. R., and R. Sivakumar, 2003: Seasonal variability of sea surface salinity and salt budget of the mixed layer of the north Indian Ocean. *J. Geophys. Res.*, **108** (C1), 3009, doi: 10.1029/2001JC000907.

Reynolds, R. W., N. A. Rayner, T. M. Smith, D. C. Stokes, and W. Wang, 2002: An improved in situ and satellite SST analysis for climate. *J. Climate*, **15**, 1609-1625.

Saji N. H., B. N. Goswami, P. N. Vinayachandran and T. Yamagata, 1999: A dipole mode in the tropical Indian Ocean. *Nature*, **401**, 360-363.

Sengupta, D., G. N. Bharath Raj, and S. S. C. Shenoi, 2006: Surface freshwater from Bay of Bengal runoff and Indonesian Throughflow in the tropical Indian Ocean. *Geophys. Res. Lett.*, **33**, L22609, doi: 10.1029/ 2006GL027573.

Sengupta, D., B. R. Goddalehundi, and D. S. Anitha, 2008: Cyclone-induced mixing does not cool SST in the post-monsoon north Bay of Bengal. *Atmos. Sci. Lett*., **9**, 1–6, doi: 10.1002/asl.162.

Shenoi, S. S. C., D. Shankar, and S. R. Shetye, 2004: Remote forcing annihilates barrier layer in southeastern Arabian Sea. *Geophys. Res. Lett.*, **31**, L05307, doi: 10.1029/2003GL019270.

Shenoi, S. S. C., V. V. Gopalakrishna, and F. Durand, 2005: Role of ocean in the genesis and annihilation of the core of the warm pool in the southeastern Arabian Sea. *Mausam.* **56**, 147–160.

Singh, O. P., T. M. Ali Khan and Md. S. Rahman, 2000: Changes in the frequency of TCs over the North Indian Ocean. *Meteor. Atmos. Phys.*, **75**, 11–20.

Singh, O. P., T. M. Ali Khan and Md. S. Rahman, 2001: Probable reasons for enhanced cyclogenesis in the Bay of Bengal during July-August of ENSO years. *Global Planet. Change*, **29**, 135–147.

Smith, R. D., J. K. Dukowicz and R. C. Malone, 1994: Parallel ocean general circulation modeling. *Physica D: Nonlinear Phenomena*, **60**, 38-61.

Sprintall, J., and M. Tomczak, 1992: Evidence of the barrier layer in the surface layer of the tropics. *J. Geophys. Res.,* **97** (C5), 7305–7316, doi: 10.1029/92JC00407.

Subrahmanyam, B., E. S. Nyadjro, C. S. Felton, G. Grunseich, and J. E. Vazquez-Cuervo, 2013: Validation of Aquarius and SMOS salinity measurements in the Indian Ocean. *IEEE Trans. Geosci. Remote Sens.* (in review).

Thadathil, P., P. M. Muraleedharan, R. R. Rao, Y. K. Somayajulu, G. V. Reddy, and C. Revichandran, 2007: Observed seasonal variability of barrier layer in the Bay of Bengal. *J. Geophys. Res.,* **112**, C02009, doi: 10.1029/2006JC003651.

Thadathil, P., and Coauthors, 2008: Seasonal Variability of the Observed Barrier Layer in the Arabian Sea. *J. Phys. Oceanogr.*, **38**, 624–638, doi: 10.1175/2007JPO3798.1.

Trenberth, K. E., 1997: The Definition of El Niño. *Bull. Amer. Meteor. Soc*., **78**, 2771–2777.

Vinayachandran, P. N., V. S. N. Murty, and V. Ramesh Babu, 2002: Observations of barrier layer formation in the Bay of Bengal during summer monsoon. *J. Geophys. Res*., **107** (C12), 8018, doi: 10.1029/2001JC000831.

Vinayachandran, P. N., D. Shankar, S. Vernekar, K. K. Sandeep, P. Amol, C. P. Neema, and A. Chatterjee, 2013: A summer monsoon pump to keep the Bay of Bengal salty. *Geophys. Res. Lett.*, **40**, 1777–1782, doi: 10.1002/grl.50274.

Yanase, W., M. Satoh, H. Taniguchi and H. Fujinami, 2012: Seasonal and Intraseasonal Modulation of Tropical Cyclogenesis Environment over the Bay of Bengal during the Extended Summer Monsoon. *J. Climate*, **25**, 2914–2930.

Yu, L. and M. J. McPhaden, 2011: Ocean Preconditioning of Cyclone Nargis in the Bay of Bengal: Interaction between Rossby Waves, Surface Fresh Waters, and Sea Surface Temperatures. *J. Phys. Oceanogr.*, **41**, 1741–1755, doi: 10.1175/2011JPO4437.1.

APPENDIX A: PERMISSION TO REPRINT

Clifford Felton <cfelton@geol.sc.edu>

Copyright Letter Request

Clifford Felton <cfelton@geol.sc.edu> Tue, Dec 17, 2013 at 11:01 AM
To: Christine Keane <ckeane@ametsoc.org>

Hello Ms. Keane,

My name is Clifford Felton, and I am a graduate student at the University of South Carolina currently working on my master's thesis. I recently published an article in the Journal of Climate and will be using it as a chapter in my MS thesis. I am the lead author on the paper and I would like to request a copyright permission letter to allow me to use my article as a chapter. The article is:

Felton, Clifford S., Bulusu Subrahmanyam, V. S. N. Murty, 2013: ENSO-Modulated Cyclogenesis over the Bay of Bengal. *J. Climate*, **26**, 9806–9818.
doi: 10.1175/JCLI-D-13-00134.1

Thank you,
Clifford Felton

--
Clifford Felton
Marine Science Program
Satellite Oceanography Laboratory
University of South Carolina
701 Sumter Street, EWS 508
Columbia, SC 29208
(803) 777-4529

Clifford Felton <cfelton@geol.sc.edu>

Copyright Letter Request

Jinny Nathans <jnathans@ametsoc.org> Tue, Dec 17, 2013 at 1:32 PM
To: cfelton@geol.sc.edu

Dear Dr. Felton—

My name is Jinny Nathans and I'm the permissions officer at AMS. This signed message constitutes permission to use the material requested in your email below.

You may use the article with the following conditions:

+ please include the complete bibliographic citation of the original source, and

+ please include the following statement with that citation: (c)American Meteorological Society. Used with permission.

Thanks very much for your request and if you need any further information, please get in touch with me. My contact information is below.

Regards,

Jinny Nathans

AMS Permissions

jnathans@ametsoc.org

617 226-3905